RESEARCH PAPER

A Revamped Element-Free Galerkin Algorithm for Accelerated Simulation of Fracture and Fatigue Problems in Two-Dimensional Domains

Ayush Awasthi[1] · Mohit Pant[1]

Abstract

This work presented a revamped element-free Galerkin method algorithm for two-dimensional fracture problems subjected to mechanical/thermoelastic loads. The conventional element-free Galerkin (EFG) technique is modified at the level of approximation along with a novel blended basis enrichment criterion together with parametric optimization at computational level. Further an optimized quadrature point criteria is embedded in the EFGM algorithm to accelerate its computational capability. The modified EFG method exhibits a higher computational efficiency and accuracy than the existing one based on moving least-squares approximation which is susceptible to generation of an ill-conditioned system of equations. The modified algorithm utilizes lesser number of nodes from the problem domain compared to the conventional EFG method for the construction of shape function. A variety of two-dimensional fracture/fatigue problems, have been modelled and simulated with the revamped algorithm. Results reveal that the revamped element-free Galerkin (REFG) method is a robust and efficient technique for modelling two-dimensional fracture problems under both mechanical and thermoelastic loads. Moreover, a significant reduction in computational time is achieved with the proposed algorithm which adds to the prowess of the proposed REFG method.

Keywords Mesh-free methods · Fracture · EFGM · Crack · Optimization

1 Introduction

Computational methods provide an edge over analytical and experimental methods by saving manpower, experimentation time and need of prototype testing. Finite element method (FEM) being one of the earliest and robust numerical tool still holds its position when it comes to solution of engineering problems. It holds the credit of being the backbone of countless engineering analysis software. This was the earliest development in computational methods for analysis of variety of problems linked with design and analysis (Afsar and Go 2010; Kaddouri et al. 2006; Ju and Hsu 2014; Chao and Chow 2002). Finite element method is a mesh-based technique hence it does not remains untouched from the limitations associated with mesh itself, for example,

problems of moving mesh boundary, phase change problems and problems involving continuous remeshing. Moreover, element distortion and low-quality mesh produce spurious results which consequentially require intensive manpower and excessive time. Mesh-free methods have been developed by the continuous improvements in the procedures of mesh-based methods. Mesh-free methods approximations are built with the use of nodal points only, and this helps in eliminating the limitations associated with mesh-based methods.

Element-free Galerkin Method (EFGM) (Belytschko et al. 1994a) is one of the mesh-free method that has been applied for analysis of a variety of problems(Belytschko et al. 1994b; Belytschko et al. 1995; Chen and Wang 2000; Xuan 2002; Li et al. 2015; Singh et al. 2003; Pathak et al. 2014). Modelling and simulations performed with EFGM depends on predefined EFG parameters like nodal density in problem geometry, Gauss quadrature used, support domain size, polynomial function used for defining the weight functions, and technique for imposing essential boundary conditions (Garg and Pant 2016).

✉ Mohit Pant
  mohitpant.iitr@gmail.com

1 Department of Mechanical Engineering, National Institute of Technology, Hamirpur, H.P. 177005, India

EFGM chalks up other mesh-free techniques used in fracture problems by eliminating the demand of remeshing and redistribution of nodal data. EFGM also enables high convergence rates and high adaptivity, and can also be applied to large distortion problems (Nguyen et al. 2008). The application of EFGM for modelling and simulating fracture problems (Pant et al. 2010, 2011a; Pathak et al. 2012; Pant and Bhattacharya 2016; Salari-Rad et al. 2011; Garg and Pant 2018a) has enabled the researchers to perform the crack analysis with a more versatile and robust tools. EFGM has emerged out as an outstanding tool for analysis of variety of problems (Garg and Pant 2018b) as it has the capability to blend with other techniques (Pathak 2017; Pathak et al. 2016, 2015, 2017). As EFGM established itself as a novel technique in the area of design and analysis, the further focus was concerned toward its modification and enhancements, so that it can be made more flexible and efficient in comparison to its conventional form.

The first advancement in EFG method started with use of moving least-square (MLS) method (Shepard 1968) for constructing the shape function and applying boundary conditions with the help of Lagrange's multiplier (Yagawa and Furukawa 2000; Belytschko et al. 1993; Günther and Liu 1998) approach. Further, there have been continuous efforts to improve the procedure for constructing the shape function (Lu et al. 1994; Wen et al. 2008) and implementing boundary conditions (Gavete et al. 2000; Lee and Yoon 2004). Ramp function was used to blend EFGM with FEM (Belytschko et al. 1995; Asadpoure et al. 2006) and fractal finite element methods (FFEM)(Rajesh and Rao 2010; Reddy and Rao 2008) to remove some inherent flaws of EFGM. Later, truly meshless technique emerged on blending EFGM with radial point interpolation method RPIM (Cao et al. 2013) as compared to coupled FEM-EFG approach. Such hybrid techniques inherited the advantages of both parent techniques to fulfil Kronecker delta property simultaneously with high-order continuity and smoothness of shape functions. Improved element-free Galerkin (IEFG) method was purposed (Kaljevic and Saigal 1997) for eliminating the singularities linked to weight functions where basis function was achieved by normalization process. An increase in computation speed in IEFG (Zhang et al. 2008) was achieved compared to the standard EFG method as lesser nodes are required for defining the domain geometry. While few researchers demonstrated the improvement of EFG method by engaging on specific parameters (Valencia et al. 2008, 2009), they did not remark on values or standards of these parameters. Wenterodt and Estorff (2011) carried out parametric analysis of various EFGM parameters like weight function, influence domain size and gauss quadrature in order to decrease the effect of dispersion in acoustics. Meshless Galerkin least-square method (MGLS) (He et al. 2011) was employed for problem based on L-shaped cavity acoustics by varying the EFGM parameters and was found that there is a significant decrement in computational time in comparison to EFGM. Computational speed was significantly increased by applying extended parametric meshless Galerkin method (Musivand-Arzanfudi et al. 2007) for simulating elastostatics problems as this method involved enrichments of approximation functions with discontinuous fields through partition of unity method. Sheng et al. (2015) proposed a criteria by employing uniform number of nodes in support domain but failed to comment about optimum number of nodes in the support domain, instead their criteria increased the total computational time of problem. The changes made in domain radius selection were flawed due to the presence of a scaling parameter (Belytschko et al. 1994a; Sheng et al. 2015; Dolbow and Belytschko 1998; Liu and Tu 2002). To the best of author's knowledge, very limited work has been emphasized on the optimum range of EFG parameters ideal for efficient simulations with least computational time. Previously performed parametric studies varied the range of EFG parameters rather than using optimization technique for multiple simulations variations.

In the present work, a novel revamped structure of element-free Galerkin algorithm has been proposed by the authors which includes:

- Use of improved moving least-square (IMLS) approximation method rather than conventional moving least-square (MLS) approximation method.
- Optimization of EFGM parameters using Taguchi's optimization to reduce the actual number of simulations required.
- Employing a newly proposed blended basis enrichment criterion rather than using conventional full basis enrichment function.
- Use of newly proposed optimized quadrature criteria for integration purpose.

The novelty of present work lies in enhancing the conventional element-free Galerkin method by blending it with Improved moving least-square method (IMLS) (Liew et al. 2005, 2006) along with optimization of EFGM parameters using Taguchi's technique into a unified EFG algorithm wherein the proposed algorithm can be used as a generic tool to model and simulate a wide variety of fracture problems with high accuracy and least computational time.

Optimization will help to choose a suitable predetermined value of the nodes (under domain of influence) thereby eliminating the confusion about suitable value of scaling parameter. Moreover, the algorithm has been blended with newly proposed enrichment criteria in order to enhance computational efficiency of the method. Algebraic equations in case of IMLS approximation are not ill conditioned and can be solved with the use of inverse matrix. Moreover,

fewer coefficients in IMLS approximation further enhance the computation speed of algorithm. The simulation so performed using the optimized parameters blended with new enrichment criteria along with improved moving least-square method (IMLS) will drastically decrease the computational time (T_{EFGM}) of EFGM analysis while keeping the accuracy intact. The new proposed algorithm is tested for various fracture problem simulations under different loadings and also in complex geometry problems. Further, the method has been extended to simulate the fatigue life estimation where the simulation needs to run for a very high number of repetitive cycles, and thus the total computational time becomes a significant parameter to be worked upon. Results reveal that the modified algorithm proposed in this article works efficiently with significantly lesser number of nodes and provide nearly 75% reduction in the computational time required for simulation.

2 EFGM Formulation for Two-Dimensional Elasticity Problems

Figure 1 shows a 2D domain bounded by Γ, subjected to various forces.

The governing equilibrium equations (Nguyen et al. 2008) are as follows:

$$\nabla . \boldsymbol{\sigma} + \mathbf{b} = 0 \quad \text{over} \, \Omega \tag{1}$$

Subjected to boundary conditions mentioned below:

$$\mathbf{u} = \bar{\mathbf{u}} \quad \text{over} \, \Gamma_u \, (\text{Essential}) \tag{2}$$

$$\boldsymbol{\sigma} . \bar{\mathbf{n}} = \bar{\mathbf{t}} \quad \text{over} \, \Gamma_t (\text{Natural}) \tag{3}$$

here $\boldsymbol{\sigma}$ represents the stress tensor, as $\boldsymbol{\sigma} = \mathbf{D}(\mathbf{x})\,[\boldsymbol{\varepsilon}]$, $\mathbf{D}(\mathbf{x})$ is the material matrix, $\boldsymbol{\varepsilon}$ is the strain vector,$\mathbf{b}$ is the body force vector, $\mathbf{u}$ is the displacement vector, $\bar{\mathbf{t}}$ is the traction force and $\bar{\mathbf{n}}$ is the unit normal. Now, using Lagrange multiplier approach (Belytschko et al. 1994a) to enforce boundary conditions and applying variational principle (Belytschko et al.
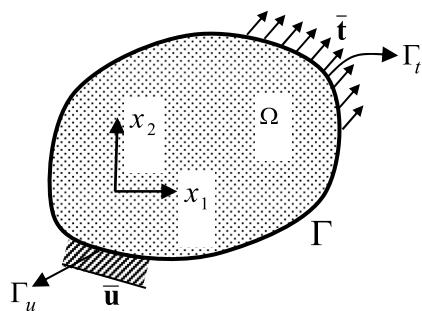

Fig. 1 Domain representation with boundary conditions

1994b; Nguyen et al. 2008), discrete equations as mentioned below is obtained from **Eq. (1)**

$$\begin{bmatrix} \mathbf{K} & \mathbf{G} \\ \mathbf{G}^T & 0 \end{bmatrix} \begin{Bmatrix} \mathbf{u} \\ \lambda \end{Bmatrix} = \begin{Bmatrix} \mathbf{f} \\ \mathbf{q} \end{Bmatrix} \tag{4}$$

where,

$$K_{IJ} = \int_{\Omega} \mathbf{B}_I^T \mathbf{D} \, \mathbf{B}_I \, d\Omega \tag{5}$$

$$f_I = \int_{\Gamma_t} \bar{\mathbf{t}} \, \Phi_I \, d\Gamma_t, \quad q_K = - \int_{\Gamma_u} \mathbf{N}_K \, \bar{u} \, d\Gamma_u \tag{6}$$

where Φ_I denotes the mesh-free shape function whose expression is derived in next section.

$\mathbf{N}_K$ is a 1D Lagrange interpolant

$$\mathbf{B}_I = \begin{bmatrix} \Phi_{I,x} & 0 \\ 0 & \Phi_{I,y} \\ \Phi_{I,y} & \Phi_{I,x} \end{bmatrix}, \quad \mathbf{N}_K = \begin{bmatrix} N_K & 0 \\ 0 & N_K \end{bmatrix}, \tag{7}$$

$$\mathbf{D} = \frac{E}{1-\nu} \begin{bmatrix} 1 & \nu & 0 \\ \nu & 1 & 0 \\ 0 & 0 & (1-\nu)/2 \end{bmatrix} \quad (\text{for plane stress})$$

$$= \frac{E}{[1+\nu][(1-2\nu)]} \begin{bmatrix} 1-\nu & \nu & 0 \\ \nu & 1-\nu & 0 \\ 0 & 0 & (1-2\nu)/2 \end{bmatrix} \quad (\text{for plane strain}) \tag{8}$$

3 Shape Function Evaluation Using Moving Least-Square (MLS) Approximation

MLS approximation used in EFGM for nodal point interpolation (Belytschko et al. 1994a, b) has been developed by Lancaster and Salkauskas (Lancaster and Salkauskas 1981). Interpolation of displacement u by MLS approximation, $u^h(x)$ is given as:

$$u^h(\mathbf{x}) = \sum_{j=1}^{m} p_j(\mathbf{x}) \, a_j(\mathbf{x}) \equiv \mathbf{p}^T(\mathbf{x}) \, \mathbf{a}(\mathbf{x}) \tag{9}$$

where m is the total number of nodes in problem domain and $\mathbf{p}^T(\mathbf{x})$ a vector of complete basis functions (usually polynomial) is given as:

$$\mathbf{p}^T(\mathbf{x}) = [1, \quad x, \quad y, \quad xy, \quad \dots \quad x^{k'}, \quad y^{k'}] \tag{10}$$

and $\mathbf{a}^T(\mathbf{x})$ is a vector of unidentified coefficients

$$\mathbf{a}^T(\mathbf{x}) = [a_1(\mathbf{x}), \quad a_2(\mathbf{x}), \quad a_3(\mathbf{x}), \dots \, a_m(\mathbf{x})] \tag{11}$$

$\mathbf{a}(\mathbf{x})$ for any location of point x can be obtained by minimizing the weighted least-square sum of the difference between local approximation, $u^h(x)$ and field function nodal parameters, u_I. This can be expressed as:

$$\mathcal{L}(x) = \sum_{I=1}^{n} w(x - x_I)\left[p^T(x)a(x) - u_I\right]^2 \tag{12}$$

$w(x - x_I)$ is the weight function linked to support domain of node I, and n represents the number of nodes within domain of influence corresponding to point x, i.e., $w(x - x_I) \neq 0$

By minimization of $\mathcal{L}$ w.r.t. a, we get:

$$M^0(x)a(x) = B^0(x)u \tag{13}$$

$$a(x) = \left(M^0\right)^{-1}(x)B^0(x)u \tag{14}$$

where $M^0(x)$ and $B^0(x)$ are defined as:

$$M^0(\mathbf{x}) = \sum_{i=1}^{n} w(x - x_I)\,\mathbf{p}(x_I)\,\mathbf{p}^T(x_I) = w(x - x_1)\begin{bmatrix} 1 & x_1 \\ x_1 & x_1^2 \end{bmatrix} + \cdots + w(x - x_n)\begin{bmatrix} 1 & x_n \\ x_n & x_n^2 \end{bmatrix} \tag{15}$$

$$B^0(\mathbf{x}) = [w(x - x_1)p(x_1), \ldots, w(x - x_n)p(x_n)] = \left\{ w(x - x_1)\begin{bmatrix} 1 \\ x_1 \end{bmatrix}, \ldots, w(x - x_n)\begin{bmatrix} 1 \\ x_n \end{bmatrix} \right\} \tag{16}$$

By using Eqs. (9) and (13), the approximation function is generated as:

$$u^h(\mathbf{x}) = \sum_{I=1}^{n} \Phi_I(\mathbf{x})u_I = \Phi^T(\mathbf{x})\mathbf{u} \tag{17}$$

where,

$$\Phi^T(\mathbf{x}) = \left\{ \Phi_1(\mathbf{x}),\ \Phi_2(\mathbf{x}),\ \Phi_3(\mathbf{x}),\ \ldots\ \Phi_n(\mathbf{x}) \right\} \tag{18}$$

$$\mathbf{u}^T = [u_1,\ u_2,\ u_3,\ \ldots\ u_n] \tag{19}$$

The mesh-free shape function $\Phi_I(\mathbf{x})$ is defined as:

$$\Phi_I(\mathbf{x}) = \sum_{j=1}^{m} p_j(\mathbf{x})\left(\left(M^0\right)^{-1}(x)B^0(x)\right)_{jI} = \mathbf{p}^T\left(M^0\right)^{-1}B_I^0 \tag{20}$$

Choice of weight function greatly affects the approximation function $u^h(\mathbf{x}_I)$ in EFG method.

4 EFGM shape Function Using Improved Moving Least-Square (IMLS) Approximation

In the MLS approximation, Eq. (13) because of ill-conditioned matrix, it sometimes becomes difficult to get the numerical solution correctly. To prevent this, Liew et al. (2005) the IMLS approximation as follows.

For $\forall f(\mathbf{x}), g(\mathbf{x}) \in \text{span}(p)$, define

$$(f, g) = \sum_{I=1}^{n} w(\mathbf{x} - \mathbf{x}_I)f(\mathbf{x}_I)g(\mathbf{x}_I). \tag{21}$$

(f, g) represents the inner product, and span($\mathbf{p}$) represents a Hilbert space.

For the set of points $\{x_i\}$ and the weight functions $\{\mathbf{w_i}\}$, if the functions $p_1(\mathbf{x})$, $p_2(\mathbf{x})$, ….. $p_m(\mathbf{x})$ in the Hilbert space span($\mathbf{p}$) satisfies the conditions:

$$(p_k, p_j) = \sum_{i=1}^{n} w_i p_k(\mathbf{x}_i)p_j(\mathbf{x}_i) \tag{22}$$

$$= \begin{cases} 0 & k \neq j \\ A_k & k = j \end{cases} \quad (k, j = 1, 2, \ldots, m),$$

Then the function set $p_1(\mathbf{x})$, $p_2(\mathbf{x})$, ….. $p_m(\mathbf{x})$ can be termed as weighted orthogonal function set with a weighted function $\{\mathbf{w_i}\}$ about points $\{x_i\}$. If $p_1(\mathbf{x})$, $p_2(\mathbf{x})$, ….. $p_m(\mathbf{x})$ are polynomials, then the function set $p_1(\mathbf{x})$, $p_2(\mathbf{x})$, ….. $p_m(\mathbf{x})$ is known as a weighted orthogonal polynomial set with weighted functions $\{\mathbf{w_i}\}$ about points $\{x_i\}$.

From Eqs. (21) and (13) are written as

$$\begin{bmatrix} (p_1, p_1)(p_1, p_2) \ldots \ldots \ldots (p_1, p_m) \\ (p_2, p_1)(p_2, p_2) \ldots \ldots \ldots (p_2, p_m) \\ \vdots \vdots \ddots \vdots \\ (p_m, p_1)(p_m, p_2) \ldots \ldots \ldots (p_m, p_m) \end{bmatrix} \begin{bmatrix} a_1(\mathbf{x}) \\ a_2(\mathbf{x}) \\ . \\ \vdots \\ a_m(x) \end{bmatrix} \cdots = \begin{bmatrix} (p_1, u_1) \\ (p_2, u_I) \\ . \\ \vdots \\ (p_m, u_I) \end{bmatrix} \tag{23}$$

If the basis function set $p_i(\mathbf{x}) \in span(p), i = 1, 2, \ldots\ldots., m,$ is a weighted orthogonal function set about points $\{x_i\}$, i.e., if $(p_i, p_j) = 0, (i \neq j),$

Then Eq. (23) becomes

$$
\begin{bmatrix}
(p_1,p_1) & 0\cdots & & 0 \\
0 & (p_2,p_2) & \cdots & \cdots & 0 \\
 & \vdots\vdots\ddots\vdots \\
00 & \cdots & \cdots & (p_m,p_m)
\end{bmatrix}
\begin{bmatrix}
a_1(\boldsymbol{x}) \\
a_2(\boldsymbol{x}) \\
. \\
\vdots \\
a_m(x)
\end{bmatrix}
\cdots\cdots = \cdots
\begin{bmatrix}
(p_1,u_I) \\
(p_2,u_I) \\
. \\
\vdots \\
(p_m,u_I)
\end{bmatrix}
\tag{24}
$$

We $a_i(\boldsymbol{x})$ can be obtained directly as:

$$
a_i(\boldsymbol{x}) = \frac{(p_i,u_I)}{(p_i,p_i)}; \dots i = 1, 2, \dots m,
$$

i.e., $\quad \boldsymbol{a}(\boldsymbol{x}) = \overline{A}(\boldsymbol{x})B(\boldsymbol{x})\boldsymbol{u}$, $\tag{25}$

where,

$$
\overline{A}(\boldsymbol{x}) = \begin{bmatrix}
\frac{1}{(p_1,p_1)}0\dots\dots 0 \\
0\frac{1}{(p_2,p_2)}\dots\dots 0 \\
\vdots\vdots\ddots\vdots \\
00\dots\dots\frac{1}{(p_m,p_m)}
\end{bmatrix}
$$

From Eqs. (25) and (9), approximation function $u^h(\boldsymbol{x})$ can be obtained as:

$$
u^h(\boldsymbol{x}) = \overline{\phi}(\boldsymbol{x})u = \sum_{I=1}^{n} \overline{\phi}_I(\boldsymbol{x})u_I
\tag{26}
$$

where $\overline{\phi}(\boldsymbol{x})$ is the shape function and

$$
\overline{\phi}(\boldsymbol{x}) = \left(\left(\overline{\phi}_1(\boldsymbol{x}), \overline{\phi}_2(\boldsymbol{x}), \dots\dots, \overline{\phi}_n(\boldsymbol{x}) \right) \right) = \boldsymbol{p}^T(\boldsymbol{x})\overline{A}(\boldsymbol{x})B(\boldsymbol{x}).
\tag{27}
$$

As coefficients $a_i(\boldsymbol{x})$ are obtained directly and simply, which eliminates the scope of obtaining an ill conditioned or singular equation system, and thus we obtain a correct solution.

From Eq. (27), we have

$$
\overline{\phi}_I(\boldsymbol{x}) = \sum_{j=1}^{m} p_j(\boldsymbol{x})[\overline{A}(\boldsymbol{x})B(\boldsymbol{x})]_{jI},
\tag{28}
$$

which represents the shape function of the **IMLS** approximation for the corresponding node **I**. We can then obtain the partial derivatives of $\overline{\phi}_I(\boldsymbol{x})$ as

$$
\overline{\phi}_{I,i}(x) = \sum_{j=1}^{m} \left[p_{j,i}\left(\overline{A}B\right)_{jI} + p_j(\overline{A}_{,i}B + \overline{A}B_{,i})_{jI} \right].
\tag{29}
$$

The weighted orthogonal basis function set $\boldsymbol{p} = (p_i)$ can be formed with the Schmidt method

$$
p_1 = 1,
$$
$$
p_i = r^{i-1} - \sum_{k=1}^{i-1} \frac{(r^{i-1},p_k)}{(p_k,p_k)}p_k, \quad i = 2, 3 \dots
\tag{30}
$$

With $r = x_1$ for one-dimensional problem, $r = \sqrt{x_1^2 + x_2^2}$ or $r = x_1 + x_2$ for two-dimensional problems, and $r = x_1^2 + x_2^2 + x_3^2$ or $r = x_1 + x_2 + x_3$ for three-dimensional problems.

In addition, the Schmidt method can be used to for the weighted orthogonal basis function set $\boldsymbol{p} = (p_i)$

$$
\overline{\boldsymbol{p}} = (\overline{p}_i) = (1, x_1, x_2, x_1^2, x_1 x_2, x_2^2, \dots),
\tag{31}
$$

Weighted orthogonal basis function set can be obtained by relation:

$$
p_i = \overline{p}_i - \sum_{k=1}^{i-1} \frac{(\overline{p}_i,p_k)}{(p_k,p_k)}p_k, i = 1, 2, 3 \dots
\tag{32}
$$

Because of weighted orthogonal basis functions, the total number of coefficients in the trial function are reduced. Less number of nodes are required in influence domain for IMLS approximation as compared to MLS approximation. This provides an edge to the IMLS approximation over the MLS approximation.

5 Blended Basis Enrichment Criteria

A new enrichment criterion has been proposed in order to enhance the computational efficiency of element-free Galerkin method (EFGM). The new enrichment criteria will be a blend of full intrinsic basis enrichment function and a linear basis function. For this, two concentric circular areas are created in the proximity of crack tip as represented in Fig. 2a. The degree of enrichment will be decided by the location of evaluation point (gauss point) under consideration, within these areas. Figure 2a demonstrates the methodology of newly proposed criteria with a schematic diagram. Two circular zones are defined having the same center. The radius of inner circle is equal to the length of crack a, while the outer circle is of radius $(c \times a)$. The value of area ratio, i.e., c^2, will be determined by performing a parametric optimization analysis for area ratio as discussed later. The three different regions are marked as A,B and C, respectively. Firstly, the location of evaluation point is obtained by calculating the distance of that evaluation point from the crack tip. If the evaluation point lies in the inner most region A, then a full intrinsic enrichment basis will be employed for imparting contribution to global stiffness matrix [**KG**] For all evaluation points lying in region C, a linear basis is used for constituting stiffness matrix.
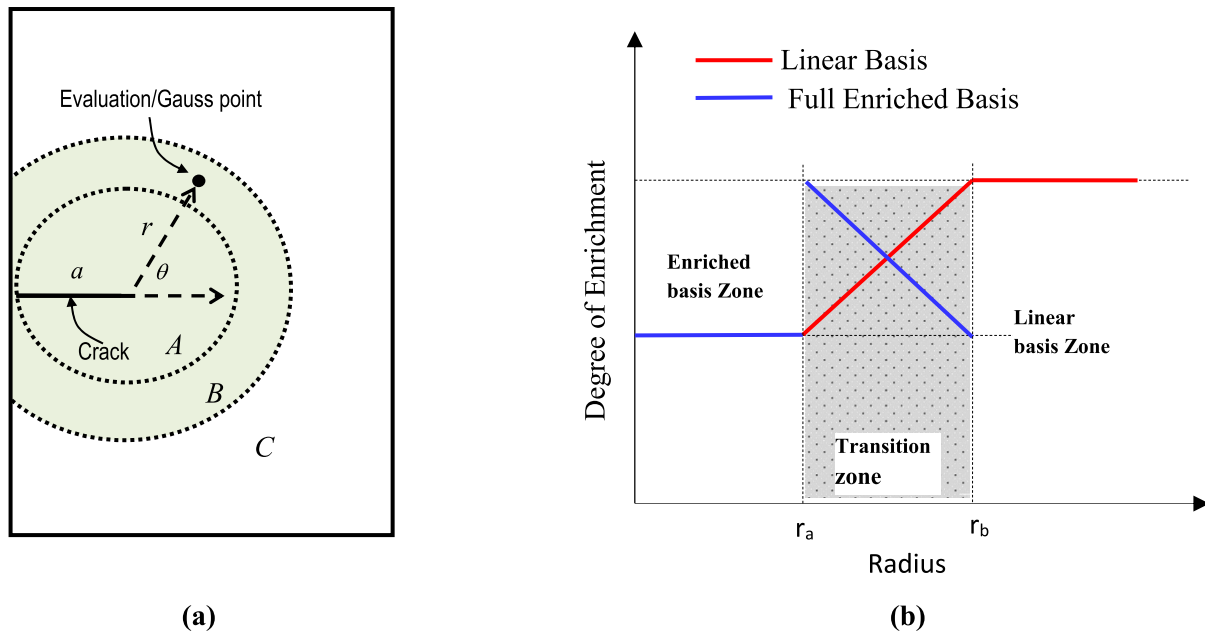
Fig. 2 Blended basis enrichment criteria **a** geometry definition and **b** degree of enrichment

But if, the evaluation point lies in the transition zone, i.e., region *B*, then instead of a sudden truncation of enrichment basis, the contribution to global stiffness matrix will be calculated using a blend of both linear and full enriched basis as follows:

$$[\mathbf{KG}]_{\text{Total}} = [\mathbf{KG}]_{\text{Enriched basis}} \times R + [\mathbf{KG}]_{\text{Linear basis}} \times (1 - R) \tag{33}$$

where the parameter *R* will decide the contribution of each basis function to the global stiffness matrix. The value of *R* can be obtained as:

$$R = \frac{(c \times a - r_g)}{(c - 1) \times a} \tag{34}$$

where *c* is a parameter which determines the area bounded within region *B*, *a* is the crack length and r_g is distance between evaluation point and crack tip. Contribution of enriched basis to the global stiffness matrix will be maximum for those points (in region B) which are nearer to the boundary of region A while contribution of linear basis will be minimum for these points. The contribution of enrichment basis continuously decreases as the location of evaluation point shifts from region *A* to region *B*. At the outer boundary of region *B*, the contribution of linear basis to the global stiffness matrix will be maximum. Figure 2b clearly illustrates the use of linear basis, full enriched basis or a combination these two according to the zone in which an evaluation point lies. The proposed criterion not only reduces the computational time of algorithm but is also capable of simulation crack tip fields in both convex and non convex domains. Figure 3 presents a flowchart for the above mentioned criterion that has been embedded in the revamped EFGM algorithm.

6 Optimized Quadrature Criteria for Integration

Stiffness matrix (**K**), displacement matrix (**G**), and force vector (**f**) are evaluated by area integration over domain in two dimensions. Gauss quadrature is required for evaluation of stiffness matrix and force vector which subdivides the domain and helps in numerical integration. Unlike finite elements, mesh-free methods do not subdivide the domain into finite elements. In order to cope with this situation, element quadrature (background mesh) is the widely used criteria for element-free Galerkin method. In conventional EFG method, a uniform Guass quadrature is employed for the entire domain. In the present work, a new optimized quadrature criteria have been proposed and employed for revamping the conventional EFG method. The proposed optimized quadrature criteria are embedded in EFG algorithm such that it is efficient in simulation both straight and kinked crack. The proposed criterion is as follows:

1. In element quadrature method, the nodal locations itself are utilized to form a background mesh of virtual elements for generation of gauss points within them. Fig-
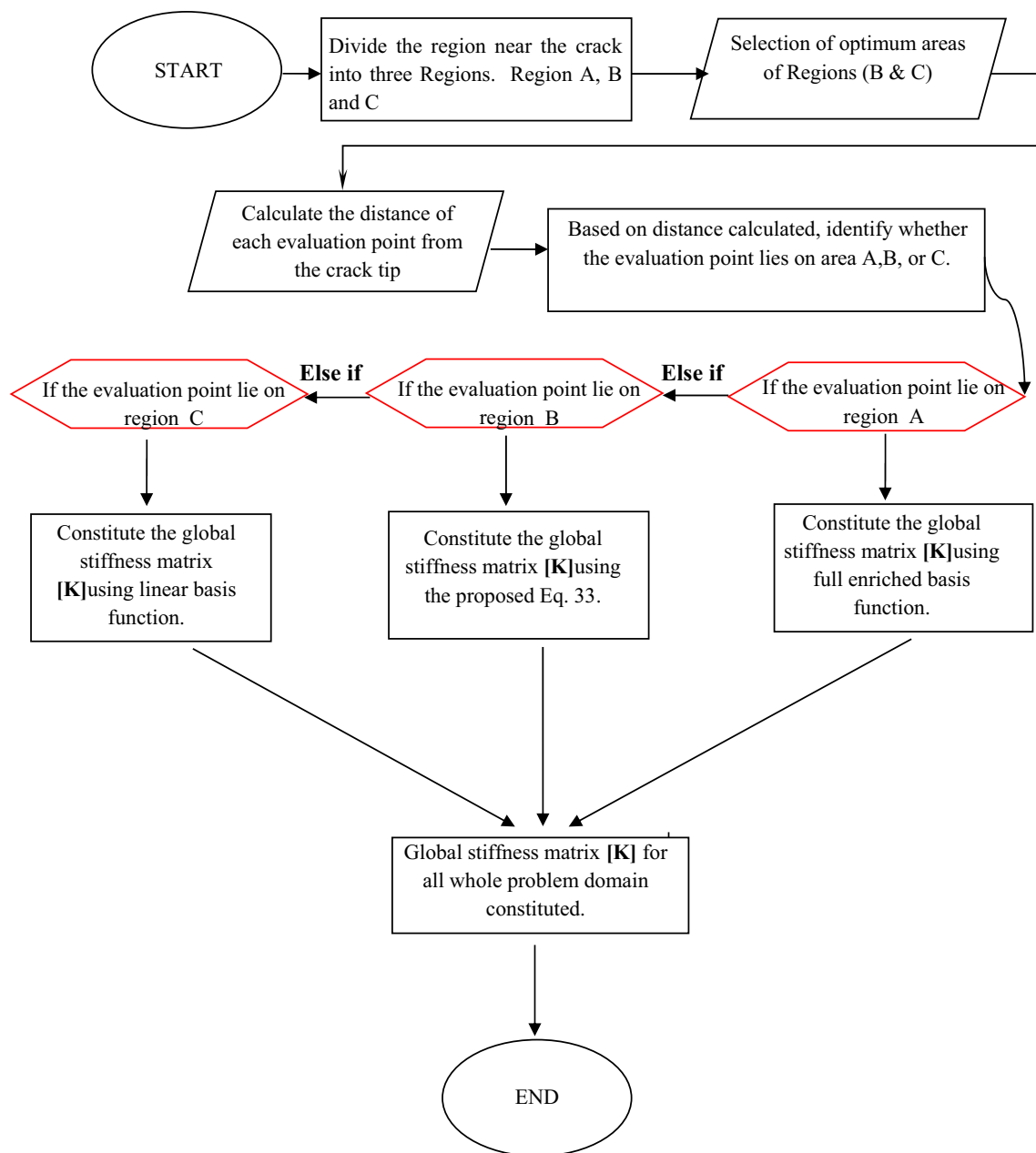
Fig. 3 Flowchart for the blended basis enrichment criteria

ure 4a shows the uniformly distributed nodes over the entire problem domain along with a crack of length *a*.

2. For a single crack, define one circular region with center at the midpoint of crack length and radius as half the crack length.

3. Define second circular region with center at the crack tip and radius as half the length of crack.

4. Select all nodes lying within these two circular domains and name them as N_E.

5. For all the virtual elements having at least one of the nodes as N_E, define a higher-order quadrature compared to the rest of domain.

As shown in Figs. 4a and 5a, the circular domains are defined by circle 1 and circle 2 and circle 3. All the virtual element lying within these two circular domains are used to define a higher-order gauss quadrature. Also the virtual elements (highlighted with star) which share at least one of the nodes from N_E are also embedded with a higher-order
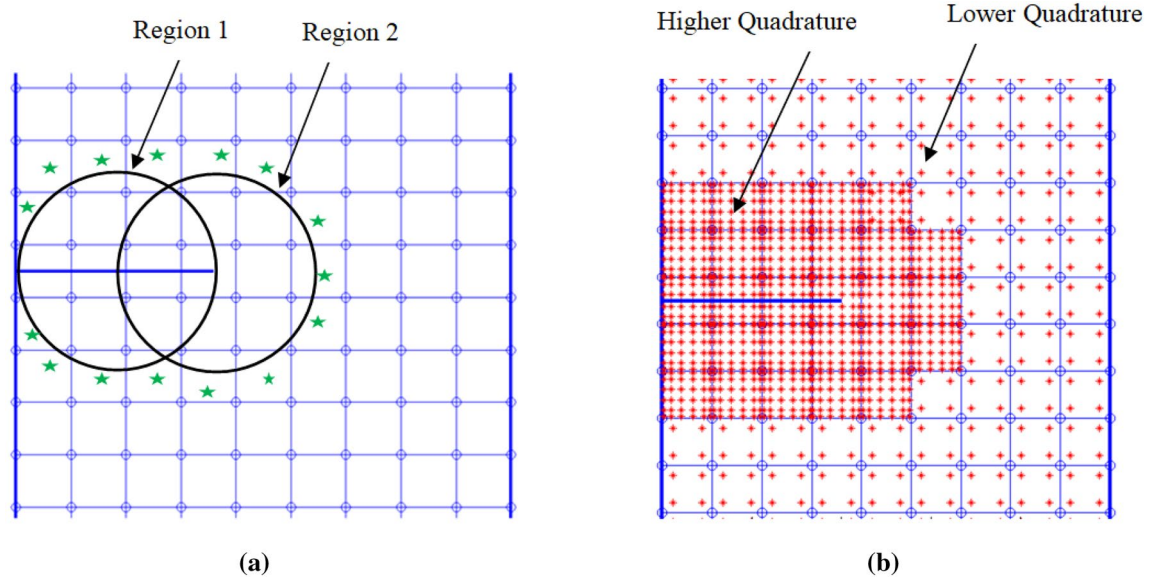
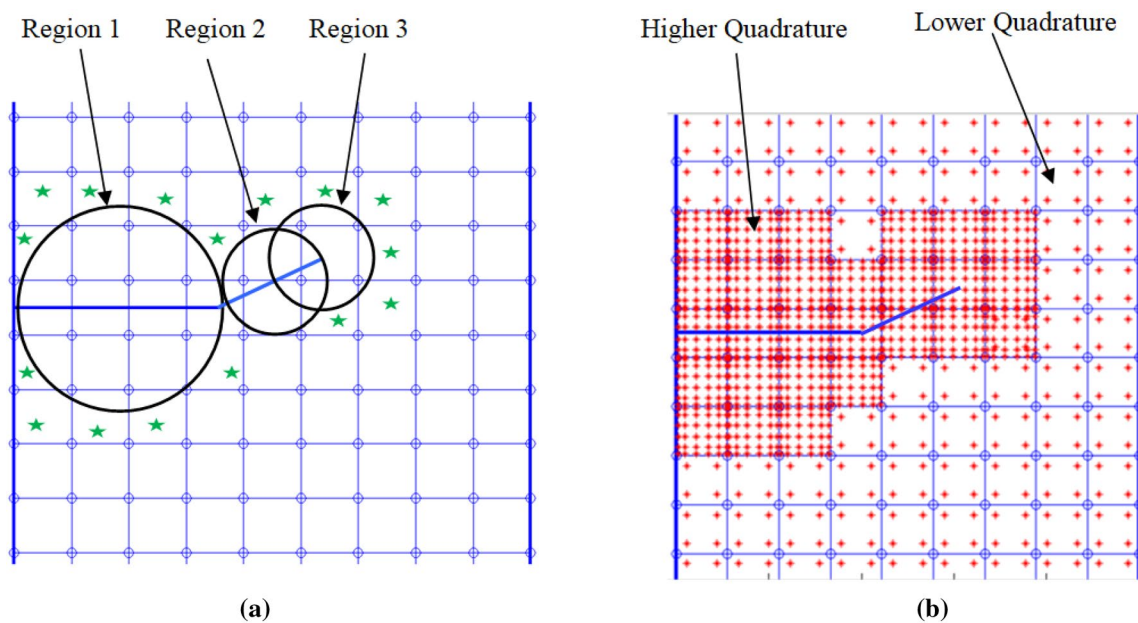**Fig. 4** Optimized quadrature criteria for straight crack

Fig. 5 Optimized quadrature criteria for kinked crack

Gaussian quadrature compared to rest of domain. Figures 4b and 5b shows the variable gauss quadrature generated inline with the above mentioned criteria. Figure 6 presents the flowchart for the proposed optimized quadrature criteria that has been embedded in revamped EFGM algorithm.

7 Modelling of Kinked Crack Segments

Near-tip asymptotic displacement field (Nguyen et al. 2008) functions are used to intrinsically enrich (Nguyen et al. 2008) the basis function of EFGM, for simulation of crack tip stress fields in fracture mechanics problems. An enriched basis (Nguyen et al. 2008) used in the present work is given as:

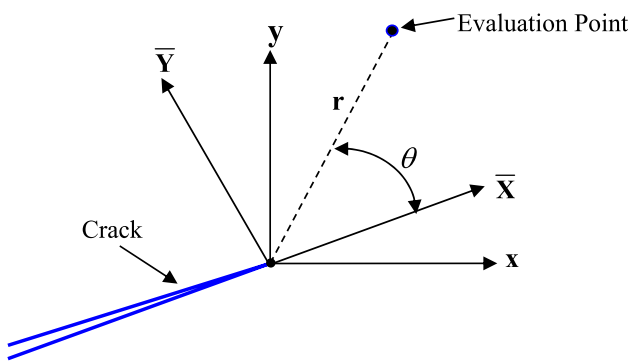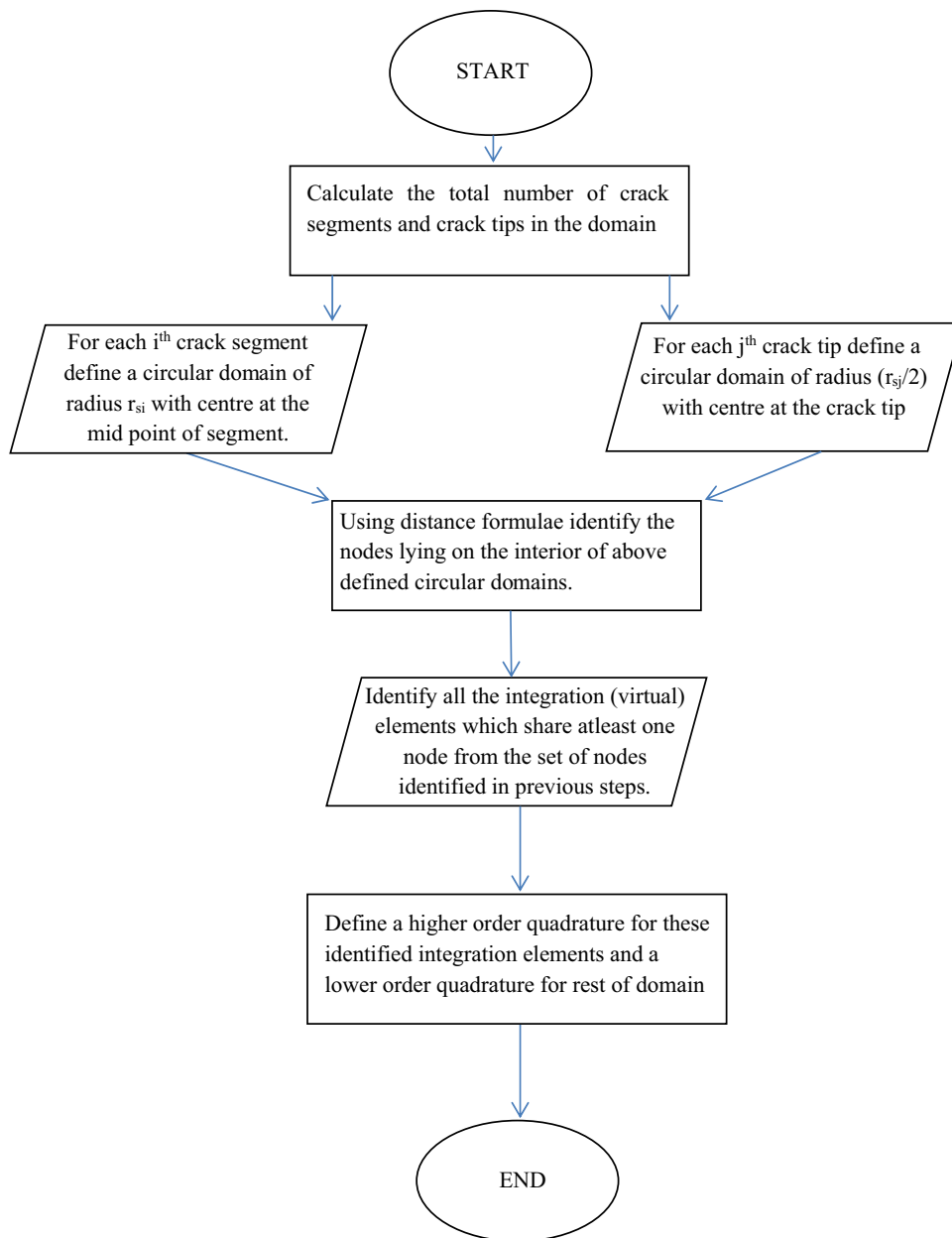**Fig. 6** Flowchart for optimized quadrature criteria

Fig. 7 Local coordinate system $(\bar{x}, \bar{y})$ at crack tip

$$\mathbf{P}^T(\mathbf{x}) = \left[1, x, y, \sqrt{r}\cos\frac{\theta}{2}, \sqrt{r}\sin\frac{\theta}{2}, \sqrt{r}\sin\frac{\theta}{2}\sin\theta, \sqrt{r}\cos\frac{\theta}{2}\sin\theta\right]$$

(35)

where r is the distance of evaluation point form the crack tip, and θ is the angle with respect to a coordinate system located at crack tip as shown in Fig. 7.

Discontinuity along $\theta = \pm\pi$ from the crack line is simulated by Eq. (35). In case of kinked crack, mapping is required for aligning the discontinuous fields with the segments of actual crack. Modification in the angular orientation of an evaluation point has been carried out, for modelling a kinked crack in the present analysis. The proposed method for modelling a kinked crack is based on the modification in angular orientation of an evaluation point. Angular
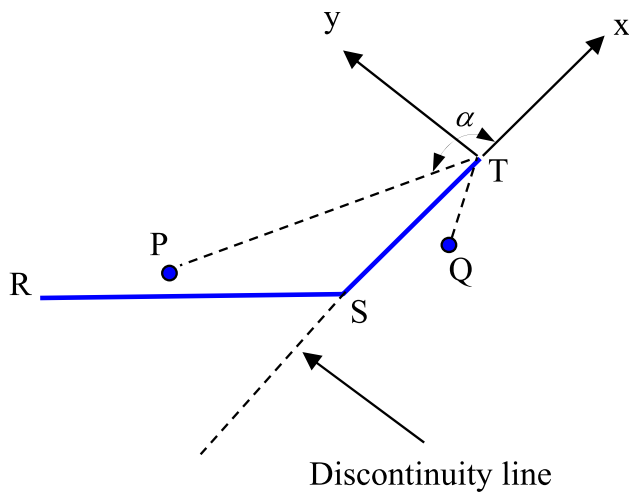
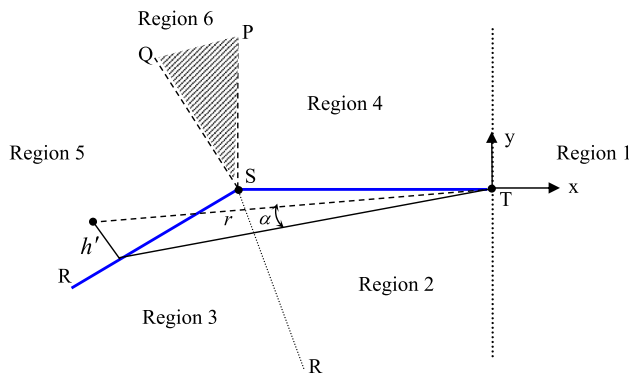**Fig. 8** Scheme for kinked crack mapping

Fig. 9 Domain description for modelling kinked crack

orientations are modified such that all the evaluation points in the proximity of crack segments exhibits a discontinuity along $\theta = \pm\pi$. *RS* and *ST* are segments of kinked crack as shown in Fig. 8. Alignment of the local coordinate system is done along the leading crack segment such that ST is aligned with x-axis having origin at the tip. Now, Consider an evaluation point *P* which is located in the vicinity of crack having the angular position α. This angular position α will require a mapping to new coordinate system where $\alpha \rightarrow \pm\pi$, in order to exhibit a discontinuity along the crack line. Mapping the angular positions of evaluation points to new coordinate system is done in way that there is discontinuity in displacement fields along the points lying near to crack line.

7.1 Methodology for Mapping a Kinked Crack

Consider a kinked crack as shown in Fig. 9. Following steps are to be followed for mapping the near-tip stress field in a kinked crack:

1. Divide the domain (containing the kinked crack) into segments like RS, *ST* where T is tip of leading crack.
2. Draw normal at common point of both segments in order to discretize the region above the crack, i.e., point B, on which normal are drawn as SQ and SP which are perpendicular to crack segments RS and ST, respectively.
3. Draw normal at tip of leading crack segment ST.
4. Draw the bisector of angle RST in order to divide the region below the crack into two parts such that a total of six regions are formed in the vicinity of kinked crack and similar procedure must be applied for cracks having multiple kinks.
5. Apply proposed geometrical and mathematical expressions to obtain the new mapped orientation of evaluation point.

In region 1 which is after the tip of leading crack, all angular measurements are done with respect to local coordinate axis, such that:

$$\theta' = \theta \ \text{ for} -\frac{\pi}{2} \le \theta \le \frac{\pi}{2} \tag{36}$$

Proposed modified angular orientation of evaluation points lying in regions 2, 3, 4 and 5 is as follows:

$$\begin{cases} \pi - \ \text{Sin}^{-1}\left(\dfrac{h'}{r}\right) & \text{above the crack} \\ -\pi + \ \text{Sin}^{-1}\left(\dfrac{h'}{r}\right) & \text{above the crack} \end{cases} \tag{37}$$

where r signifies the distance between tip of the leading crack i.e. Point T and the evaluation point, h' signifies the normal distance between the crack segment in that region and the evaluation point. For points inside the region QSP and h' is calculated as the distance between the evaluation point and point representing that region, i.e., Point S. In performing so, a transformation achieved as point approaches to the crack line such that $h' \rightarrow 0$ then $\theta' \rightarrow \pm\pi$, and thus clear discontinuity is achieved along the crack line.

Hence, the new enriched basis function in term of modified angular orientation θ' becomes:

$$\mathbf{P}^T(\mathbf{x}) = \left[\underbrace{1,\ x,\ y}_{\text{standard basis}},\ \underbrace{\sqrt{r}\cos\frac{\theta'}{2},\ \sqrt{r}\sin\frac{\theta'}{2},\ \sqrt{r}\sin\frac{\theta'}{2}\sin\theta',\ \sqrt{r}\cos\frac{\theta'}{2}\sin\theta'}_{\text{enrichment terms}} \right] \tag{38}$$

where, $(1, x,y)$ that is the first three terms represents standard basis and the rest four terms composes of enrichment part for the kinked crack.

8 Interaction Integral Approach for Calculating Stress Intensity Factors

The J-integral for a isotropic cracked body is as follows (Rao and Rahman 2003):

$$J = \int_{\Gamma} \left(W\delta_{ij} - \sigma_{ij}\frac{\partial u_i}{\partial x_1} \right) n_j d\Gamma \tag{39}$$

where $W = \int_0^{\varepsilon}\sigma d\varepsilon$ is the strain energy density, σ is the stress and n is outward unit normal vector to a discretional curve surrounding the crack tip as shown in Fig. 10. For linear elastic materials,$W = \sigma_{ij}\varepsilon_{ij}/2$. Green's theorem (Rao and Rahman 2003) can be applied to covert contour integral in Eq. 39 into area integral.

$$J = \int_A \left(\sigma_{ij}\frac{\partial u_i}{\partial x_1} - W\delta_{ij} \right)\frac{\partial q}{\partial x_j} dA \tag{40}$$

where A represents the area under the curve and q is a weight function, which has zero value along the boundary of domain and unity at the crack. Now assume two states for a cracked body, State 1 which is primary state or real state having some predefined boundary conditions and the other state 2 which is a secondary or auxiliary state. The J-integral in the superimpose states is as follows:

$$J^U = \int_A \left[\left(\sigma_{ij}^{(1)} + \sigma_{ij}^{(2)} \right)\frac{\partial\left(u_i^{(1)} + u_i^{(2)} \right)}{\partial x_i} - W^U\delta_{ij} \right]\frac{\partial q}{\partial x_j} dA \tag{41}$$

where $i, j = 1, 2$, and U specifies fields and quantities associated with primary, secondary and unified states, respectively.

On expanding Eq. (41):

$$J^U = J^{(1)} + J^{(2)} + M^{(U)} \tag{42}$$

where

$$M^{(U)} = \int_A \left[\sigma_{ij}^{(1)}\frac{\partial u_i^{(2)}}{\partial x_1} + \sigma_{ij}^{(2)}\frac{\partial u_i^{(1)}}{\partial x_1} - W^U\delta_{ij} \right]\frac{\partial q}{\partial x_j} dA \tag{43}$$

This is interaction integral which is employed for computing stress intensity factors (SIFs) under mechanical loads. Thermal interaction integral for homogeneous materials under the thermal loading is precisely elaborated by Pant et al. (2010) as follows:

$$M^{(U)} = \int_A \left[\sigma_{ij}^{(1)}\frac{\partial u_i^{(2)}}{\partial x_1} + \sigma_{ij}^{(2)}\frac{\partial u_i^{(1)}}{\partial x_1} - W^U\delta_{ij} \right]\frac{\partial q}{\partial x_j} dA + \alpha\int_A\frac{\partial T}{\partial x_1}\sigma_{kk}^2 q\, dA \tag{44}$$

Here, the terms represented in bold are the additional terms that are needed for thermal interaction integral calculation. T represents Temperature applied, α is thermal expansion coefficient and σ_{kk} is the thermal stress.

Fig. 10 Crack surrounded by area A_o
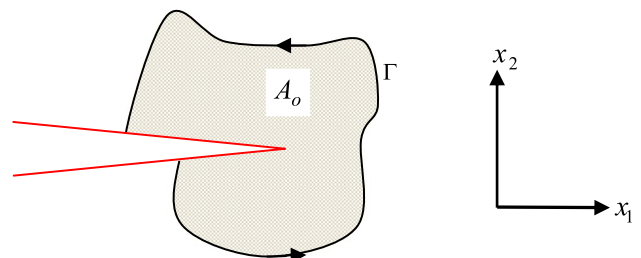
9 Results and Discussion

This section presents optimization of EFGM parameter along with implementation of proposed algorithm to model and simulate few numerical problems of fracture and fatigue life estimation. The revamped EFG algorithm incorporates:

- IMLS approximation.
- Blended enrichment criteria.
- Optimized quadrature criteria
- Criteria for modelling kinked crack.

The application of the revamped EFGM algorithm has been demonstrated for a variety of fracture problems with different geometric and loading conditions. Finally, proposed the method has been extended to simulate fatigue crack growth problem in order to establish its worth and robustness for efficiently reducing the computation time.

9.1 Parametric Optimization

The number of nodes in problem domain (n_d), order of Gauss quadrature, scaling factor (d_{max}) and area ratio (c^2) influences the total time of EFGM simulation. Earlier parametric studies (Musivand-Arzanfudi et al. 2007; Sheng et al. 2015) on EFGM were mainly focused on multiple number of simulations (range 600–1000) instead of using some optimization technique. Taguchi optimization (Kosaraju et al. 2012) technique has been applied in current work and L16 orthogonal array has been selected for the analysis which in turn reduces the actual number of simulations required for
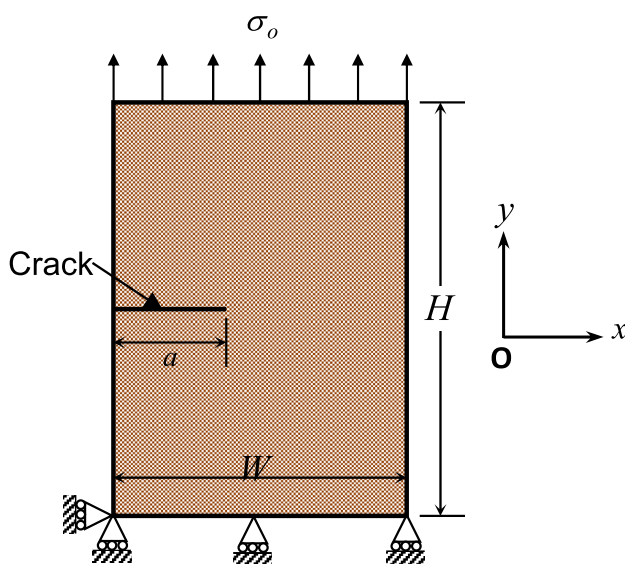

Fig. 11 Problem geometry along with boundary conditions

Table 1 Process parameters and their levels for Taguchi design of experiments

Process parameters	Symbol	Levels			
		I	II	III	IV
Total number of nodes (n_d)	A	200	800	1800	3200
Gauss quadrature	B	2×2	4×4	6×6	8×8
Scaling factor d_{max}	C	1.5	2	2.5	3
Area ratio	D	1.5	2	2.5	3

finding the optimum parameters, thus providing the computationally efficient form of EFGM.

Optimization technique is applied here for analysis of an edge crack problem with different EFGM parameters. In this Taguchi analysis (Kosaraju et al. 2012; Mahapatra and Patnaik 2007; Wang et al. 2016; Elizalde-Gonzalez and Garcia-Diaz 2010) relative deviation has be considered as the response value for the analysis. In the current optimization analysis, four parameters namely, total number of nodes, gauss quadrature type, scaling factor (d_{max}), and area ratio (A_r) are selected as the input parameters for finding the optimum combination of these parameters for simulations.

For finding the optimum values of these parameters, a cracked rectangular domain having height $(H) = 2$ units and width $(W) = 1$ units and having mechanical properties $(E = 1 \times 10^6 \text{units}, v = 0.3)$ subjected to tensile load of $\sigma_0 = 1$ unit, under plane stress conditions is selected for this study as shown in Fig. 11.

Crack orientation is parallel to the horizontal axis located at coordinates $x = 0$ and $y = H/2$ and a size of $a = 0.4$ units.

The variable range of parameters used in the present analysis are: Number of nodes ranging from 200–300, gauss quadrature ranging from order of 2*2 to 8*8, Scaling factor (d_{max}) from 1.5 to 3 and area ratio (c^2) ranging from 1.5 to 3. Table 1 represents the various control parameters along with their respective levels. Sixteen simulations analysis have been performed as per the Taguchi's L-16 orthogonal array (Elizalde-Gonzalez and Garcia-Diaz 2010). Results of simulation are shown in Table 2. The values of Mode-I stress intensity factor (SIF) values thus obtained, are compared with Ref. 1 (Salari-Rad et al. 2011) results and the relative deviation is calculated using: $\left(RD = \left| \left(\frac{K_1^{\text{Ref.1}} - K_1^{\text{EFGM}}}{K_1^{\text{Ref.1}}} \right) \times 100 \right| \right)$.

MINITAB 17 software has been used for the Taguchi's design of experiments and optimization analysis. All EFGM simulations are performed using algorithm written in MATLAB coding platform with HP workstation having Xeon (Quad-core)-CPU with 16 GB RAM.

Signal-to-noise (S/N) ratio for the results have been calculated using MINITAB 17 software. Taguchi's characteristic of "*minimum is better*" is applied in the present analysis, as a less relative deviation is required for our simulations,

Table 2 L16 Orthogonal array for experimentation along with response outputs

L16 (4^4)	A	B	C	D	K_I (EFGM)	K_I Ref. 1	RD (%)	S/N ratio (db)
1	200	2×2	1.5	1.5	1.7418	2.3570	26.100	− 28.3331
2	800	4×4	2	1.5	2.454	2.3570	4.1196	− 12.2972
3	1800	6×6	2.5	1.5	2.369	2.3570	0.4921	6.1580
4	3200	8×8	3	1.5	2.4309	2.3570	3.1353	− 9.9257
5	1800	4×4	1.5	2	2.3437	2.3570	0.5642	4.9702
6	3200	2×2	2	2	2.1604	2.3570	8.3411	− 18.4245
7	200	8×8	2.5	2	2.4542	2.3570	4.1238	− 12.3061
8	800	6×6	3	2	2.3554	2.3570	0.0678	23.3648
9	3200	6×6	1.5	2.5	2.6303	2.3570	11.595	− 21.2856
10	1800	8×8	2	2.5	2.2488	2.3570	4.5905	− 13.2374
11	800	2×2	2.5	2.5	2.3233	2.3570	1.4297	− 3.1054
12	200	4×4	3	2.5	2.7230	2.3570	15.590	− 23.8603
13	800	8×8	1.5	3	2.8605	2.3570	21.361	− 26.5928
14	200	6×6	2	3	2.5248	2.3570	7.1192	− 17.0486
15	3200	4×4	2.5	3	2.359	2.3570	0.7636	2.3417
16	1800	2×2	3	3	2.0028	2.3570	15.027	− 23.5378

Fig. 12 Plot for mean of S/N ratios
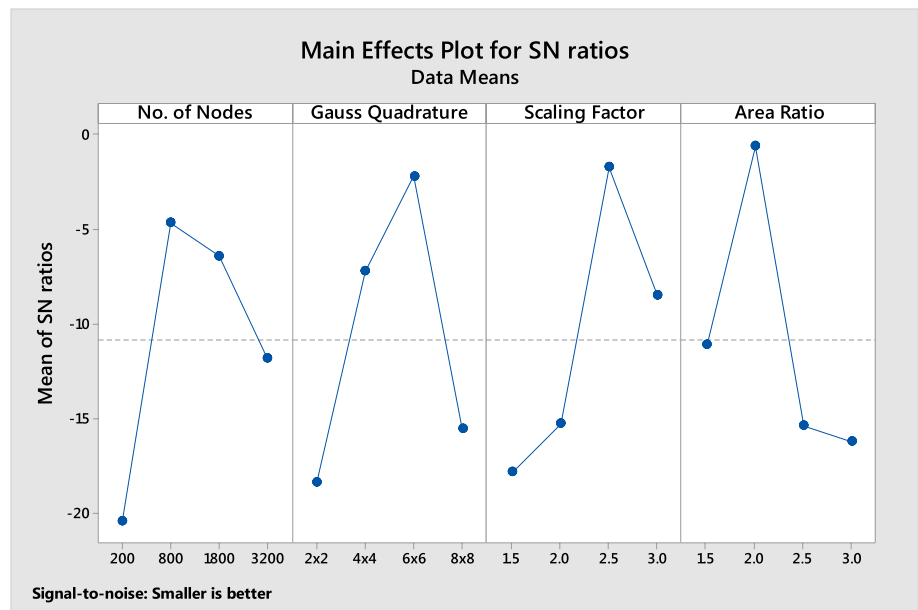
Table 3 Computational time comparison

Process parameters	Method	
	Conventional EFGM	Revamped EFGM
Number of nodes (n_d)	800	800
Gauss quadrature	6×6	Variable
Scaling factor (d_{max})	2.5	2.5
Area ratio	–	2
Computational time	110 s	22 s

to obtain optimum results. The loss function L for objective is defined as follows:

$$L_{LB} = \frac{1}{n} \sum_{i=1}^{n} y_{RD}^2 \qquad (45)$$

where y_{RD} is the value of relative deviation (RD) and n is number of experiments.

Signal-to-noise ratio can also be calculated by logarithmic transformation as follows:

$$\text{S/N ratio for relative deviation} = -10 \log_{10} \left(L_{\text{LB}} \right) \quad (46)$$

The effect of control parameters on relative deviation is shown in Table 2. Figure 12 shows the mean of S/N ratio with the condition that minimum is better. Plot reveals that the control factors at levels A_2, B_3, C_3, and D_2 contribute maximum in obtaining low relative deviations, and thus, they may be regarded as the optimum levels for carrying out further simulations.

Next, the simulations at these corresponding optimum levels have been performed; using proposed revamped element-free Galerkin method (REFGM), to calculate the values of K_{I} and relative deviation. Value of $K_{\text{I}} = 2.3365$ units and a relative deviation of 0.85% were observed and time consumed for this simulations was found to be 22 s.

In order to have a relative comparison of the computational time, the same problem was simulated using conventional EFGM approach. All other simulation parameters were kept same as shown in Table 3. A relative comparison of computational time predicts that the revamped element-free Galerkin method (REFGM) is faster than the conventional method by 80% with nearly equal accuracy of results.

The revamped EFG method is further employed for modelling of a variety of fracture and fatigue problem to ensure and establish its accurate simulation capabilities with least computational time.

9.2 Bimetallic Interfacial Cracks

Both conventional EFGM and revamped EFGM have been employed for solving bimaterial interface crack problems.

Jump function (Pant et al. 2011b) has been used to model the material discontinuity, i.e., weak discontinuity and intrinsic enrichment (Nguyen et al.2008) has been used to model the strong discontinuities. Interaction integral (Sukumar et al. 2004; Yau et al.1980) in domain form has been used for calculating the stress intensity factors as follows:

$$M = - \int_A \left(\sigma_{ik} \varepsilon_{ik}^{aux} \delta_{1j} - \sigma_{ij} u_{i,1}^{aux} - \sigma_{ij}^{aux} u_{i,1} \right) \overline{q}_j \, \mathrm{d}A \quad (47)$$

where, $\overline{q}$ is a weight function which has zero value on the contour C and unity at the tip of crack. Relation between stress intensity factor and integration integral is given as (Sukumar et al. 2004):

$$M_i = \frac{2}{E^* \cosh^2(\pi \tilde{\varepsilon})} (K_{\text{I}} K_{\text{II}}^{aux} + K_{\text{I}} K_{\text{II}}^{aux}) \quad \text{with } i = 1, 2 \quad (48)$$

K_{I}^{aux} and K_{II}^{aux} are auxiliary stress intensity factors and E^* is equivalent Young's Modulus ($E^* = 2E_1 E_2 / (E_1 + E_2)$) and $\tilde{\varepsilon}$ is the bimaterial constant (Sukumar et al. 2004). K_{I}^{aux} can be calculated by considering $K_{\text{I}}^{aux} = 1$ and $K_{\text{II}}^{aux} = 0$, and similarly K_{II} can also be calculated.

A bimetallic rectangular plate having a Width $W = 100$ mm and Height, $H = 200$ mm, with an interface crack located at the center has been considered for analysis, as shown in Fig. 13a. Horizontal material interface is located at a distance of $H/2$ from the bottom of plate. A tensile load of 9.8 MPa has been applied perpendicular to the interface of the crack. A nodal density of (20×50) nodes is used to define the problem domain. Near-tip nodal arrangement and selection of higher quadrature regions are shown in Fig. 13b. As per the optimized quadrature criteria discussed in previous section, all the cells lying within the circular
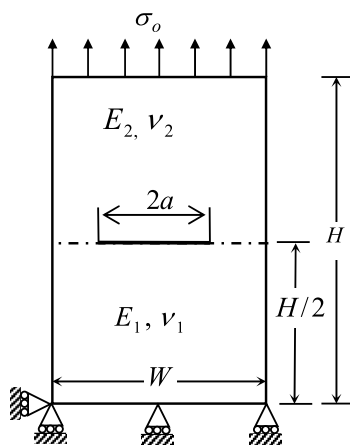
(a) Bi-metallic plate with an interface crack
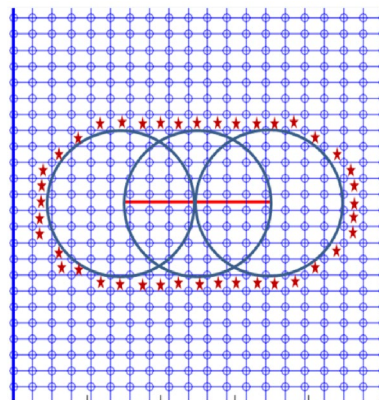
(b) Nodes and optimized quadrature cells

Fig. 13 **a** Bimetallic plate with an interface crack, **b** nodes and optimized quadrature cells
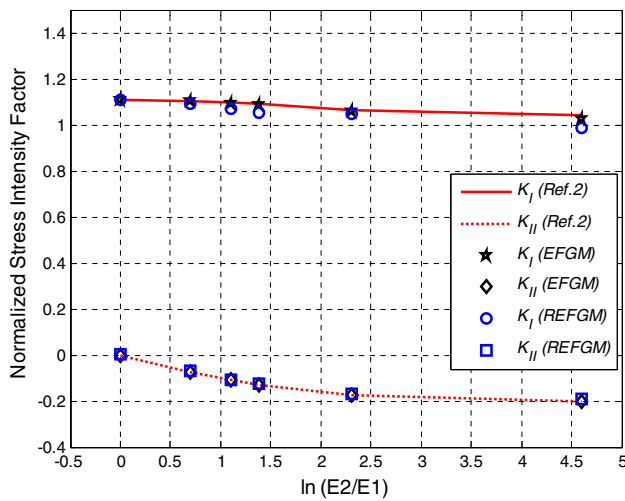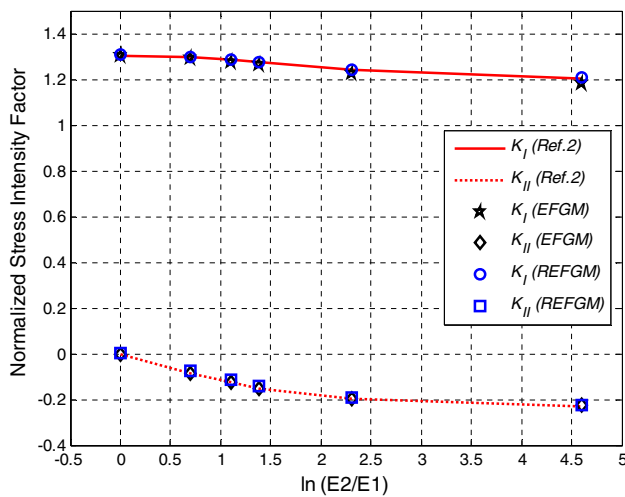
Fig. 14 SIFs variation for $2a = 40$ mm

Fig. 15 SIFs variation for $2a = 60$ mm

regions along with partially intersected cells (highlighted with star) will employ a higher Gaussian quadrature (6×6) as compared to the rest of domain having a (4×4) Gaussian quadrature.

Cracks with different lengths, i.e., 40 mm and 60 mm, are considered in the present analysis. Poisson's ratio for both materials is taken as 0.3 and value of Young's modulus (E_1) for lower material is fixed at 205.8 GPa while that of upper material (E_2) is varied. For different ratio of Young's modulus, i.e., $E_2/E_1 = 1, 2, 3, 4, 10, 100$, the values of stress intensity factors are calculated.

The normalized stress intensity factor is defined as $K_i / \sigma \sqrt{\pi a}$ ($i = 1, 2$). This is done so as to get a non-dimensional value of stress intensity factor corresponding to both mode-I and mode-II stress intensity factors. The results were compared with those obtained by Ref. 2 (Miyakazi et al. 1993; Nagashima et al. 2003). Variation of normalized stress intensity factors corresponding to varying modular ratio E_2/E_1 for a crack length of 40 mm is shown in Fig. 14. A good agreement has been found between the REFGM results and the reference results. Next simulation has been performed for a crack length of 60 mm, and the results were compared with the Ref. 2 (Miyakazi et al. 1993; Nagashima et al. 2003) as shown in Fig. 15. Tables 4 and 5 show comparison of the values of normalized stress intensity factors for various material mismatch ratios with the reference values along with comparison of simulation time of the proposed REFGM algorithm with the conventional EFGM results.

Further, the revamped EFGM algorithm was utilized to generate the contours of σ_{YY} and ε_{YY} for large material mismatch ratio at the interface, i.e., $E_2/E_1 = 100$. In this case, the stress contours of σ_{YY} is almost continuous as shown in Fig. 16a while strain contours of ε_{YY} shows a discontinuity at the interface as shown in Fig. 16b. Table 6 presents a comparison of average computational time of REFGM algorithm for simulation of bimetallic interfacial crack problem with respect to conventional EFGM technique. It can be clearly observed that the revamped EFGM algorithm is capable of reducing the average computational time by 76%.

9.3 Fracture in Functionally Graded Material

A cracked plate made of functionally graded material with properties varying as hyperbolic tangent function have been

Table 4 Normalized of stress intensity factors for crack length 40 mm

E2/E1	K$_I$ (Ref. 2)	K$_{II}$ (Ref. 2)	K$_I$ (EFGM)	K$_{II}$ (EFGM)	K$_I$ (REFGM)	K$_{II}$ (REFGM)	T$_{EFGM}$ (s)	T$_{REFG}$ (s)
1	1.111	0.000	1.095	0.000	1.1032	0.000	120	27
2	1.104	−0.073	1.0924	−0.0718	1.110	−0.076	118	29
3	1.096	−0.0109	1.0703	−0.1064	1.095	−0.011	117	28
4	1.089	−0.130	1.0531	−0.1263	1.087	−0.110	121	27
10	1.066	−0.173	1.0465	−0.1669	1.065	−0.176	124	30
100	1.039	−0.203	0.9856	−0.1942	1.037	−0.200	119	28

Table 5 Normalized of stress intensity factors for crack length 60 mm

E2/E1	K_I (Ref 2)	K_{II} (Ref 2)	K_I (EFGM)	K_{II} (EFGM)	K_I (REFGM)	K_{II} (REFGM)	T_{EFGM} (s)	T_{REFG} (s)
1	1.305	0.000	1.308	0.000	1.307	0.000	117	29
2	1.296	−0.085	1.299	−0.077	1.295	−0.084	125	27
3	1.284	−0.127	1.289	−0.116	1.282	−0.125	115	27
4	1.273	−0.150	1.273	−0.139	1.275	−0.152	113	28
10	1.239	−0.198	1.242	−0.189	1.238	−0.195	120	28
100	1.201	−0.228	1.207	−0.226	1.202	−0.229	127	30

Fig. 16 σ_{xx} and ε_{xx} contours for $E_2/E_1 = 100$

(a)

(b)
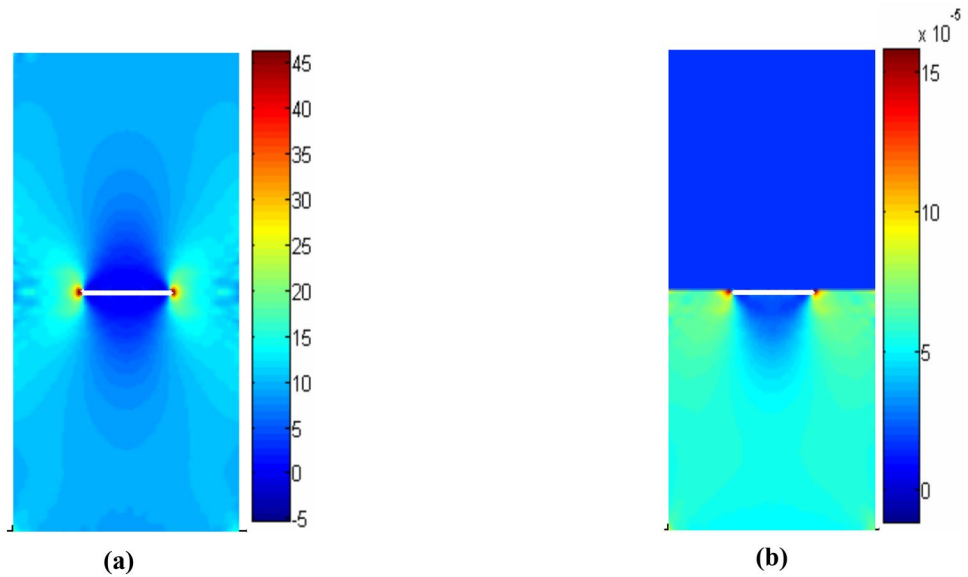
Table 6 Computational time comparison for crack in bimaterial domain

Process parameters	Method	
	Conventional EFGM	Revamped EFGM
Total number of nodes (n_d)	1000	1000
Gauss quadrature	6 × 6	Variable
Scaling factor (d_{max})	2	2
Area ratio	–	2
Average computational time	120 s	28 s

analyzed in this section. Dimensions of this functionally graded plate having an edge crack of length a are width = 2 units and height = 4 units as shown in Fig. 17a. Constraints are applied in y-direction for both top and bottom edges. Steady state thermal loadings in form of temperatures $T_1 = -10\,°C$ and $T_2 = 0\,°C$ is applied to the plate. Top and bottom edges are considered to be insulated so that there is no heat flux across them. Plane strain condition has been assumed to simulate this problem along a uniform distribution of 1250 nodes. The values of Young's modulus (E),

Poisson's ratio (v), thermal expansion coefficient (β), and thermal conductivity (k) are obtained by its hyperbolic tangent function as:

$$E(X_1) = \frac{E^- + E^+}{2} + \frac{E^- - E^+}{2} \tanh\left[\tilde{\delta}(X_1 + d)\right] \tag{49}$$

$$v(X_1) = \frac{v^- + v^+}{2} + \frac{v^- - v^+}{2} \tanh\left[\hat{\delta}(X_1 + d)\right] \tag{50}$$

$$\beta(X_1) = \frac{\beta^- + \beta^+}{2} + \frac{\beta^- - \beta^+}{2} \tanh\left[\hat{\delta}(X_1 + d)\right] \tag{51}$$

$$k(X_1) = \frac{k^- + k^+}{2} + \frac{k^- - k^+}{2} \tanh\left[\hat{\delta}(X_1 + d)\right] \tag{52}$$

w h e r e $(E^-, E^+) = (1, 3)$, $(v^-, v^+) = (0.3, 0.1)$, $(\beta^-, \beta^+) = (0.01, 0.03)$, $(k^-, k^+) = (1, 3)\tilde{\delta} = 15$, $\hat{\delta} = 5$, $d = 0$. The steady state temperature distribution over the problem domain has been generated and shown in Fig. 17b. The near-tip nodal distribution along with optimized quadrature cells for defining higher quadrature is shown in
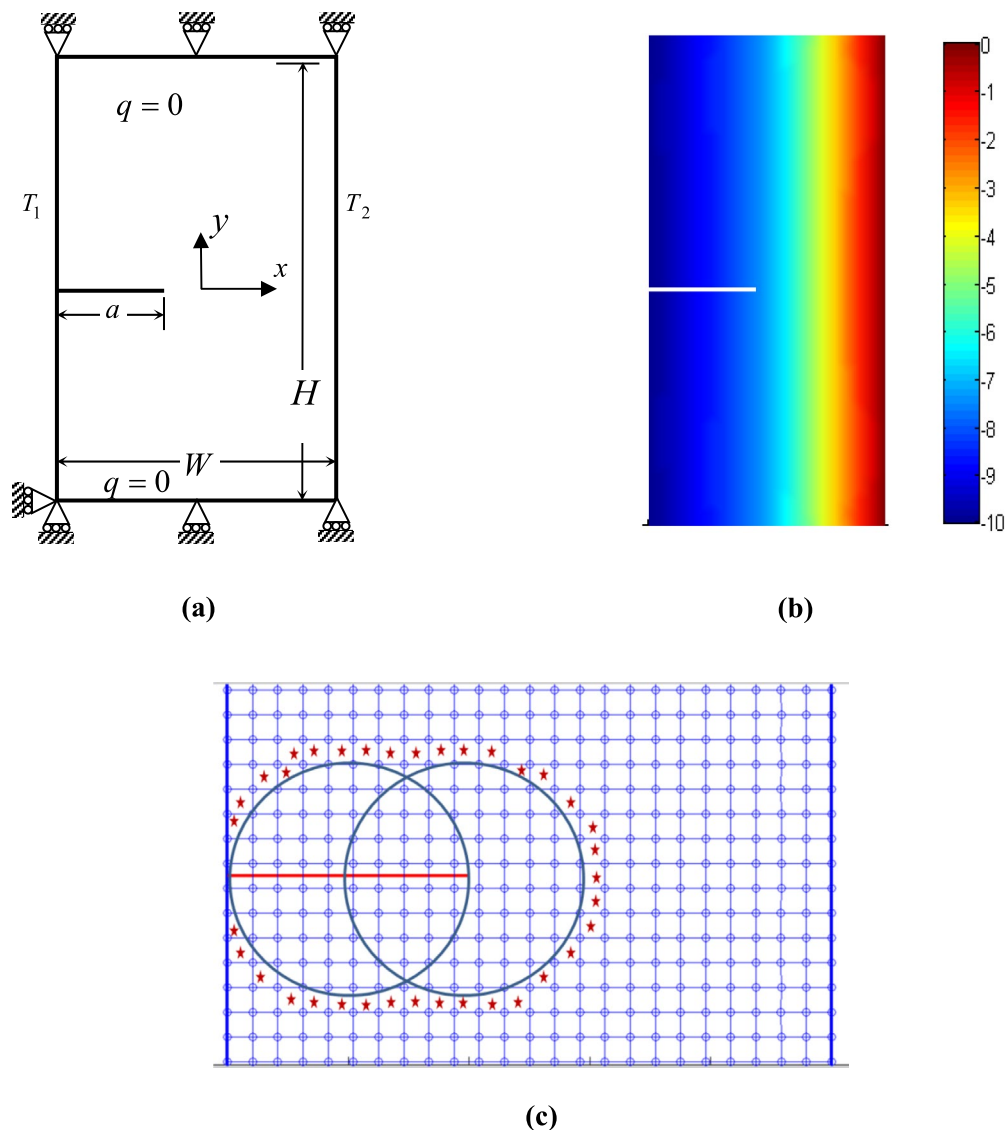
Fig. 17 **a** Problem geometry, **b** temperature distribution over the domain, **c** nodes and optimized quadrature cells

Fig. 17c. As proposed by the optimized quadrature criteria, the cells lying within the circular regions along with the boundary cells (highlighted with star) will employ a higher Gaussian quadrature compared to the rest of domain. Equations (49–52) are plotted to visualize the gradation of material properties across the width and a sharp jump in these material properties has been observed at the mid of width as shown in Figs. 18 and 19.

By analyzing the displaced nodal positions from Fig. 20a, it has been observed that edge crack exhibited only mode 1 displacements under these prescribed loading and boundary conditions.

For different $\left(\frac{a}{W}\right)$ ratios, the mode-I stress intensity factor has been plotted as shown in Fig. 20b, a good agreement can be seen between the obtained REFGM results and reference FEM solution (Kc et al. 2008). A decrement in the value of K_I, with increasing crack length (due to the gradation in material properties) has been observed. Table 7 shows a comparison of mode-I stress intensity factors and computational time for both EFGM and REFGM algorithm with the FEM reference values. It can be clearly observed that REFGM algorithm is capable of generating accurate results with least computational time for simulation of interfacial crack domain problem in comparison to conventional EFGM scheme. Moreover, a comparison of average computational time reveals that revamped EFGM algorithm is faster than its predecessor EFGM method by around 75% as shown in Table 8.
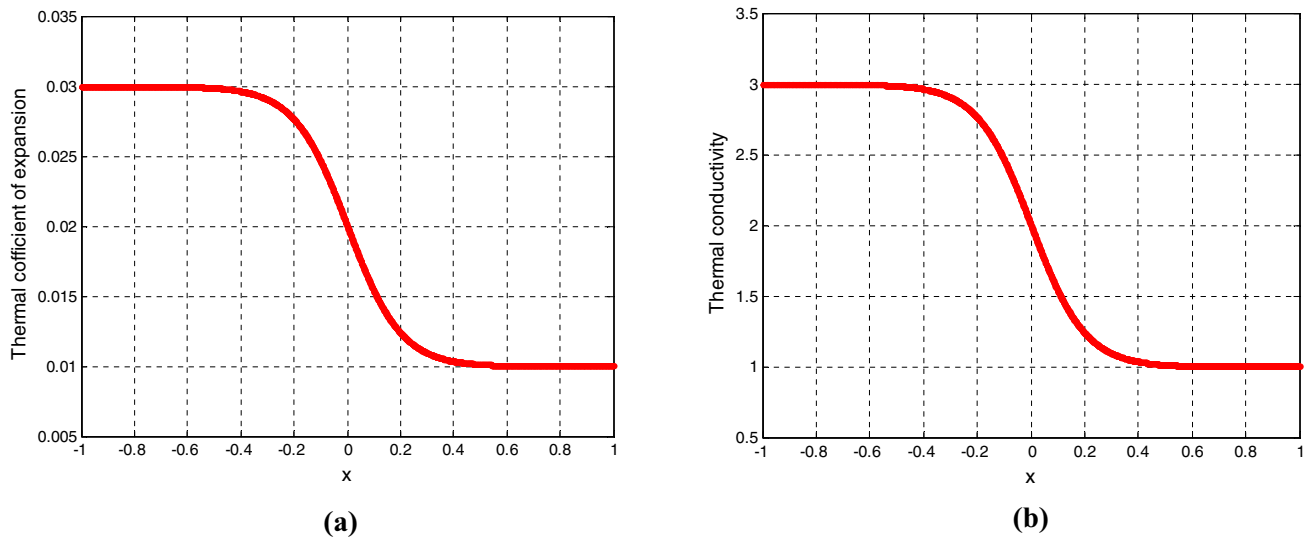
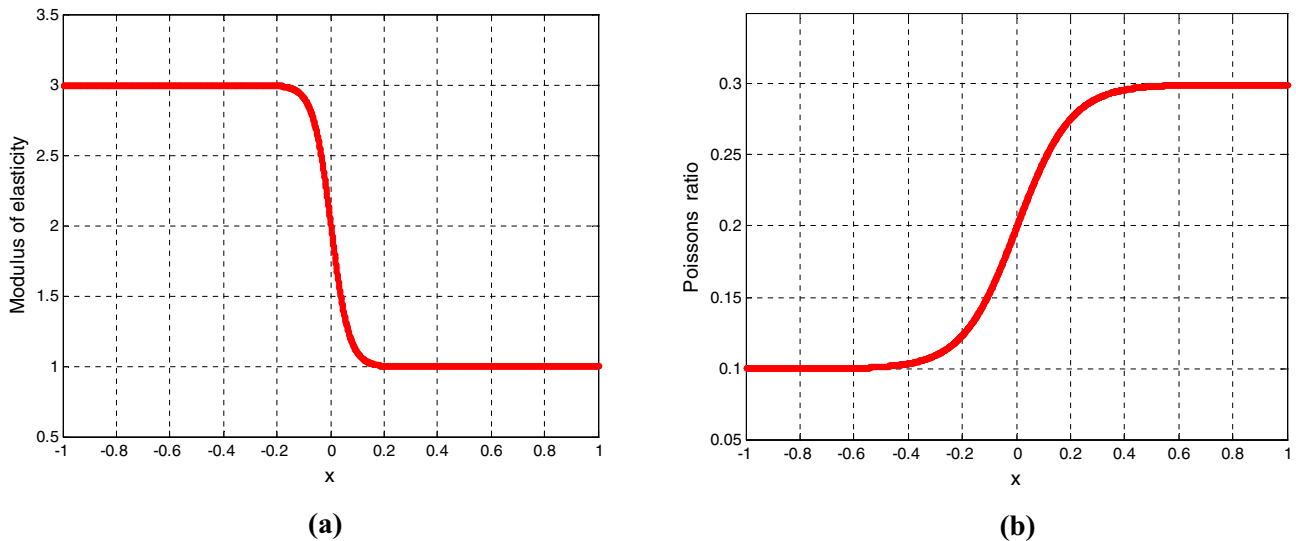**Fig. 18** Gradation of coefficient of thermal expansion and thermal conductivity across the width

Fig. 19 Gradation of modulus of elasticity and Poisson's ratio across the width

9.4 Thermoelastic Fracture

This section describes the application of REFGM for simulation of fracture problems under thermoelastic loading. At first, the temperature distribution over the cracked domain is obtained by solving the heat transfer equation across the domain. The temperature field so obtained is then employed as an input to determine the nodal displacements and near-tip stress fields.

In the present simulation, a rectangular plate of dimensions width = 5 units and height = 1 units containing inclined adiabatic crack (Pant et al. 2010) as shown in Fig. 21a has been analyzed. Uniform discretization of the plate geometry

has been done by taking 32 nodes in x direction and 64 nodes in y-direction. Top and bottom edges of this rectangular plate were kept at equal and opposite temperatures ($T_1 = 10\,°C$), while right and left edges were kept insulated so that there is not heat flow across them and crack surface is considered adiabatic. Discontinuous temperature field is observed at the center of the plate as shown in Fig. 21b.

Next, a rectangular plate of dimensions width = 1 units and height = 2 units containing isothermal center crack (Pant et al. 2010) as shown in Fig. 22a has been analyzed. Uniform nodal density has been used to define the domain by considering 32 nodes in x direction and 64 nodes in y-direction. All edges of the rectangular plate has been kept at same
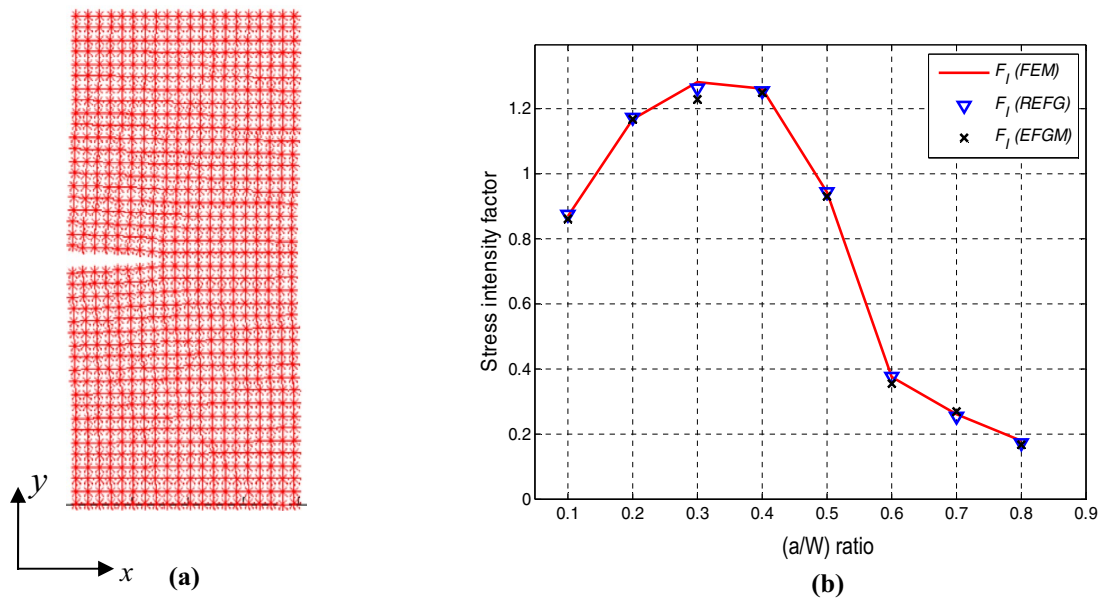
Fig. 20 Displaced nodal positions and variation of stress intensity factor

Table 7 Comparison of stress intensity factors and computational time

a/W	K_I (FEM)	K_I(EFGM)	K_I(REFGM)	T_{EFGM} (s)	T_{REFG} (s)
0.1	0.8713	0.8619	0.8723	124	33
0.2	1.1700	1.1670	1.1710	129	34
0.3	1.2840	1.2320	1.2640	132	31
0.4	1.2620	1.2520	1.2540	129	34
0.5	0.9417	0.9317	0.9437	121	36
0.6	0.3737	0.3537	0.3727	137	29
0.7	0.2588	0.2688	0.2498	136	31
0.8	0.1774	0.1674	0.1714	137	30

Table 8 Comparison of average computational time

Process parameters	Method	
	conventional EFGM	Revamped EFGM
Total number of nodes (n_d)	1250	1250
Gauss quadrature	6×6	Variable
Scaling factor (d_{max})	2	2
Area ratio	–	2
Computational time	130 s	32 s

temperature ($T_2 = 10°C$)), while temperature of the crack surface has been kept at ($T_1 = 0°C$)) such that $T_1 < T_2$. As can be seen from Fig. 22b continuous temperature field has been observed since the crack surface having a prescribed

temperature value is considered as a part of essential boundary.

The value of stress intensity factors K_I and K_{II} have been calculated using the modified thermal interaction integral (Pant et al. 2010). The normalization of stress intensity factors is done by by $\beta \, \Theta \, (W/H) E \sqrt{2W}$ for the adiabatic crack and $\beta \left(T_2 - T_1 \right) E \sqrt{2W}$ for the isothermal crack (Pant et al. 2010), where E is the Young's modulus of elasticity, ν is the Poisson's ratio, β is the coefficient of linear expansion, $\Theta = T_o - T$ with T_o is the applied temperature and T is the ambient temperature.

Figures 21c and 22c represent the near crack tip arrangements of nodes and implementation of optimized quadrature criteria for both adiabatic and isothermal crack modelling, respectively. For a particular angular orientation of the crack circular regions are defined as stated in optimized quadrature criteria. For this particular case all the cells lying within circular regions along with partially intersected cells (highlighted with star) are determined as shown in Figs. 21c and 22c. A higher Gaussians quadrature is employed for all such cells, while a lower Gaussian quadrature is used for rest of the domain.

Variation of normalized stress intensity factor for an adiabatic crack with respect to inclination angle is shown in Fig. 23a. Figure 23a shows that value of mode-I stress intensity factor is zero at inclination angle $\alpha = 0°$ and 90° and maximum at inclination angle of 45°, while value of mode-II stress intensity factor is found maximum at inclination angle of 0° and decreases to zero for inclination angle 90°. It has been seen that the calculated values of K_I and K_{II} are in good agreement with the results of literature Ref. 3 (Prasad and
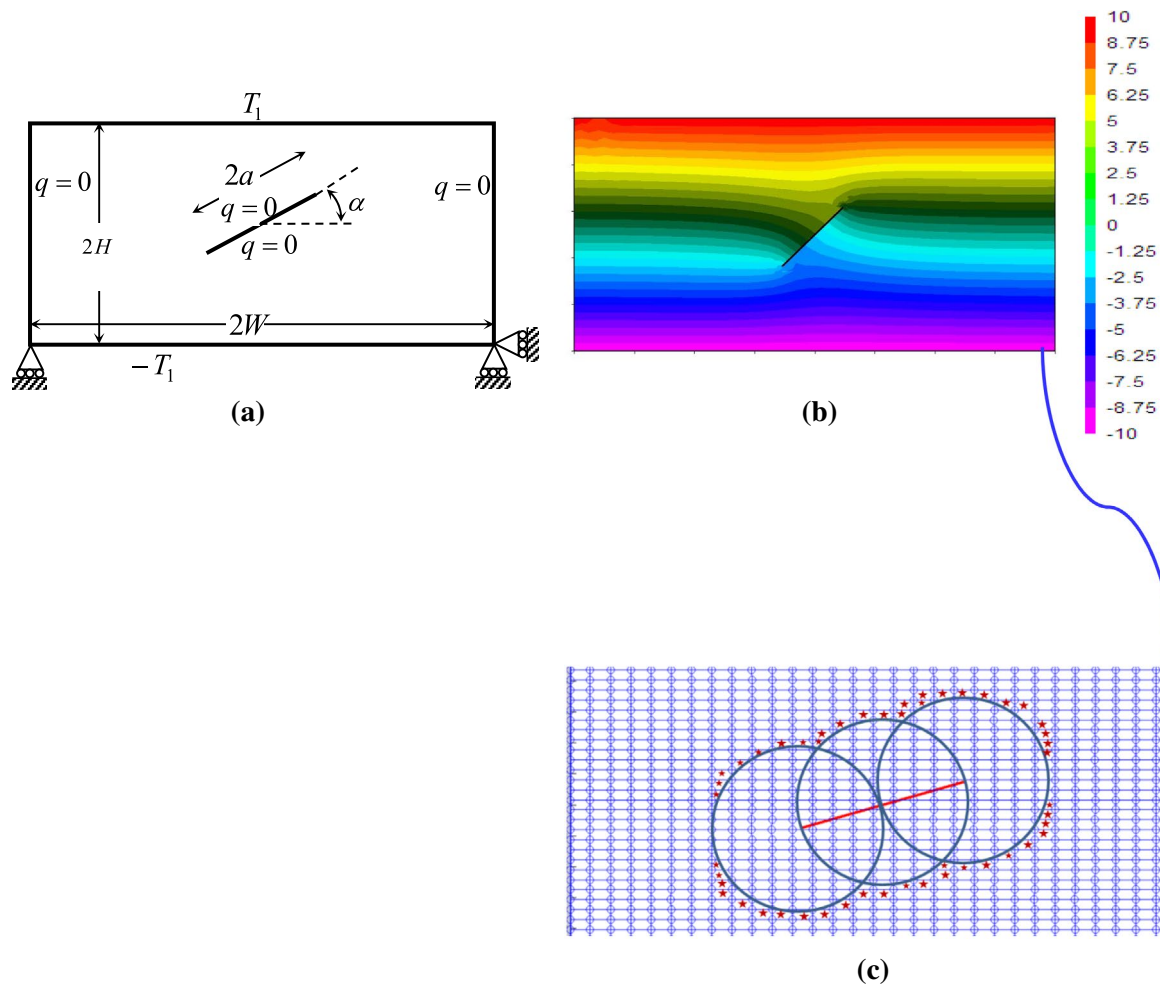
Fig. 21 Adiabatic inclines crack: **a** problem geometry, **b** temperature profile

Aliabadi 1994; Duflot 2008). Table 9 represents the variation of normalized stress intensity factors with varying crack inclination along with a comparison of simulation time for conventional EFG technique and proposed REFG algorithm.

Variation of normalized stress intensity factor for an isothermal crack with respect to inclination angle is shown in Fig. 23b. Value of both mode-I stress intensity factor and mode-II stress intensity factors has been calculated. Figure 23b shows that the value of mode-I stress intensity factor decreases from its maximum value at angle $\alpha = 0°$ to a minimum value at 90°, while value of mode-II stress intensity factor is found maximum at inclination angle of 45° and decreases to zero for inclination angle $\alpha = 0°$ and 90°. It has been seen that the calculated values of K_I and K_{II} are found in good agreement with the results of literature Ref. 3 (Prasad and Aliabadi 1994; Duflot 2008). Table 10 represents the variation of normalized stress intensity factors with varying crack inclination along with a comparison of conventional EFGM technique and proposed REFGM algorithm in terms of computational efficiency. Results show that

algorithm is quiet faster than the EFGM technique without any compromise in accuracy of results.

Table 11 represents a comparison of average computational time for thermoelastic problems simulated using both EFGM and REFGM algorithm with same parameters. The proposed REFGM algorithm has an edge over the computational time by about 76% as compared to EFGM algorithm.

9.5 Fatigue Crack Growth

Finally, a fatigue crack growth analysis for a two-dimensional homogeneous cracked domain is performed under a cyclic mechanical loading of fixed amplitude. Paris law has been used to calculate fatigue life cycles for each crack increments. The change in stress intensity factor (ΔK) for constant cyclic loads is as follows:

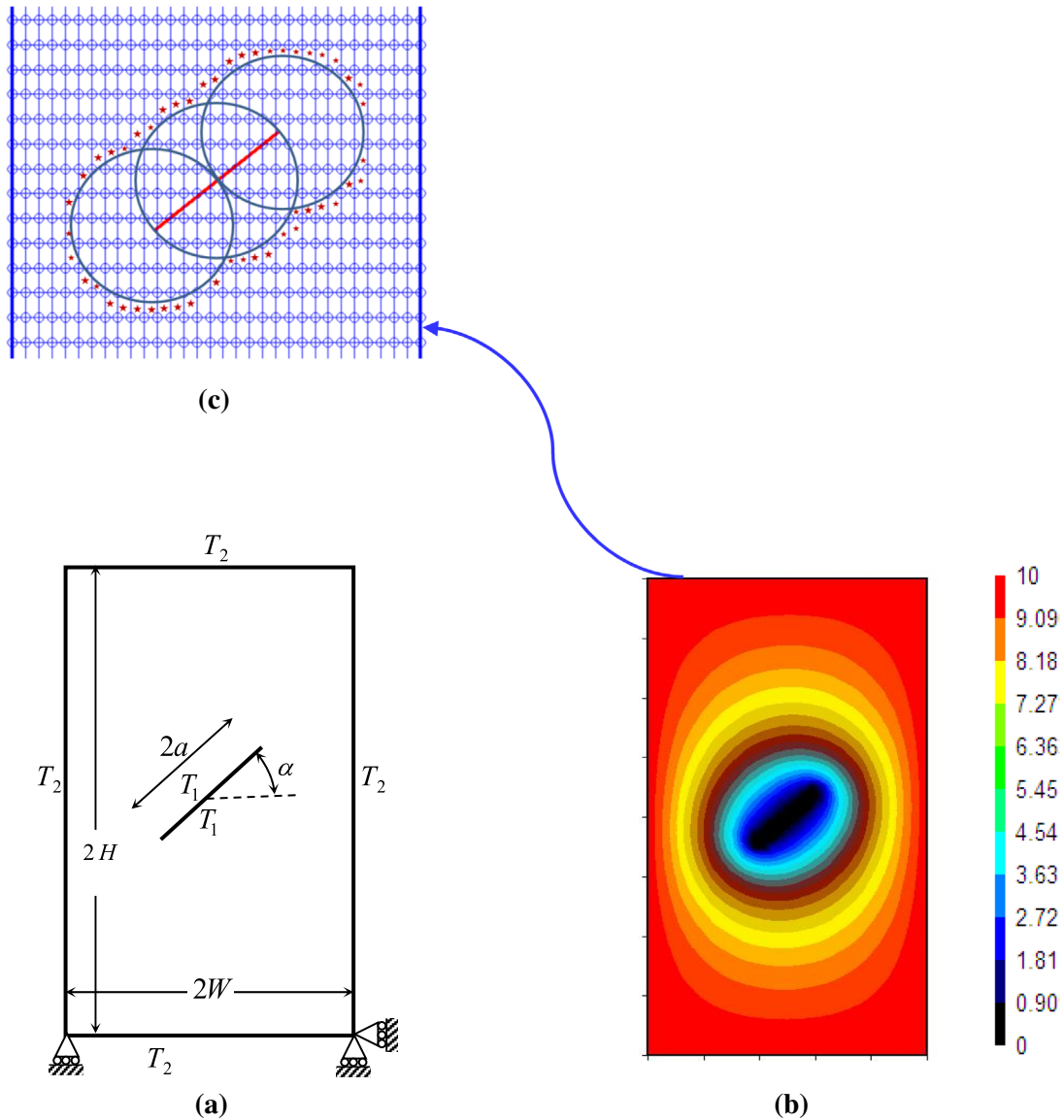$$\Delta K = K_{\text{maximum}} - K_{\text{minimum}} \tag{53}$$

Fig. 22 Isothermal inclines crack: **a** problem geometry, **b** temperature profile

where $K_{maximum}$ is the stress intensity factor corresponding to maximum applied load (σ_{max}) and $K_{minimum}$ is the stress intensity factor corresponding to minimum applied load (σ_{min}). Small linear increments of crack have been used in current work for modelling quasistatic crack growth. At the crack tip, the local direction of crack growth θ_c is determined on the basis of maximum principal stress theory (Sukumar and Prevost 2003). So, direction for the crack growth θ_c is obtained from relation:

$$K_I \sin \theta_c + K_{II}(3 \sin \theta_c - 1) = 0 \tag{54}$$

Simplifying above equation, we obtain

$$\theta_c = 2 \tan^{-1} \left(\frac{K_I - \sqrt{K_I^2 + 8K_{II}^2}}{4K_{II}} \right) \tag{55}$$

From Eq. (55), we get two values of θ_c, out of which one is the maximum value. ΔK_{Ieq} can be calculated using Eq. (54) by using the value of θ_c corresponding to maximum equivalent stress intensity factor and is written as follows:

$$\Delta K_{Ieq} = \Delta K_I \cos^3 \left(\frac{\theta_c}{2} \right) - 3\Delta K_{II} \cos^2 \left(\frac{\theta_c}{2} \right) \sin \left(\frac{\theta_c}{2} \right) \tag{56}$$
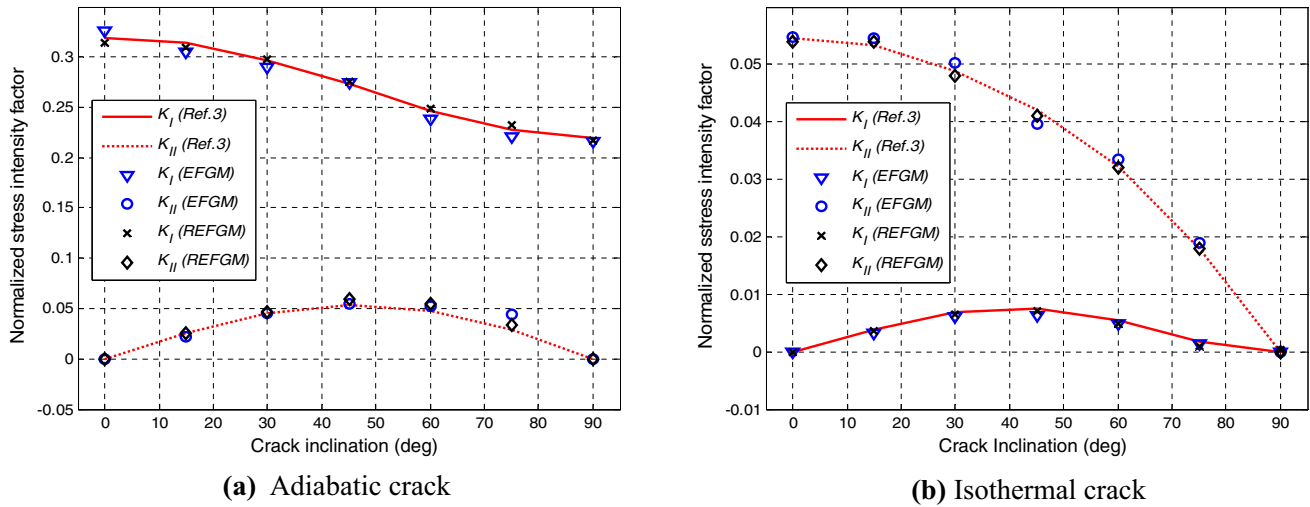
(a) Adiabatic crack   **(b)** Isothermal crack

Fig. 23 Variation of normalized stress intensity factor with crack inclination

Table 9 Variation of normalized stress intensity factors with crack inclination for adiabatic crack

θ	K_I (Ref. 3)	K_{II} (Ref. 3)	K_I (EFGM)	K_{II} (EFGM)	K_I (REFGM)	K_{II} (REFGM)	T_{EFGM} (s)	T_{REFG} (s)
0	0.319	0.000	0.3261	0.000	0.314	0.000	214	52
15	0.314	0.026	0.3047	0.022	0.310	0.025	215	54
30	0.297	0.045	0.2892	0.0451	0.298	0.047	213	33
45	0.273	0.054	0.2750	0.0549	0.276	0.059	216	51
60	0.247	0.048	0.2380	0.0520	0.249	0.055	212	54
75	0.228	0.029	0.2205	0.0439	0.232	0.034	215	53
90	0.220	0.0	0.2156	0.0	0.217	0.0	213	53

Table 10 Variation of normalized stress intensity factors with crack inclination for isothermal crack

θ	K_I (Ref. 3)	K_{II} (Ref. 3)	K_I (EFGM)	K_{II} (EFGM)	K_I (REFGM)	K_{II} (REFGM)	T_{EFGM} (s)	T_{REFG} (s)
0	0.0	0.0546	0.0	0.0548	0.0	0.002	212	53
15	0.0038	0.0533	0.0031	0.0545	0.0036	0.054	216	51
30	0.0068	0.0489	0.0060	0.0502	0.0064	0.048	213	50
45	0.0076	0.0420	0.0062	0.0397	0.0071	0.041	211	54
60	0.0054	0.0322	0.0049	0.0334	0.0049	0.032	215	53
75	0.0017	0.0180	0.0014	0.019	0.0010	0.018	216	49
90	0.0	0.0	0.0	0.0	0.0	0.0	213	52

Paris law is applied for calculating fatigue life of a propagating quasi-static crack under cyclic loading using the following expression:

$$\frac{\mathrm{d}a}{\mathrm{d}N} = C(\Delta K_{Ieq})^m \tag{57}$$

where a represents length of crack, N is number of load cycle, m and C are material constants of Paris model. Crack length is modified after obtaining the direction and magnitude of crack increment. For crack growth simulations we require optimum value of crack extension as larger crack increments will not represent real path of crack. Simulations for fatigue crack growth problems are provided with increment of 1 mm (optimum increment size). Table 12 shows the material properties considered for calculation of fatigue life.

9.5.1 Fatigue Crack Growth an Inclined Edge Crack

A problem domain with dimensions 100 mm × 200 mm with an inclined edge crack has been considered for fatigue

Table 11 Comparison of average computational time for thermoelastic problems

Process parameters	Method	
	conventional EFGM	Revamped EFGM
Total number of nodes (n_d)	2048	2048
Gauss quadrature	6×6	Variable
Scaling factor (d_{max})	2	2
Area ratio	–	2
Computational time	212 s	50 s

Table 12 Material properties for fatigue life calculation

S. no	Parameter	Numerical value
1	Elastic modulus of plate (E)	200 GPa
2	Poisson ratio (ν)	0.3
3	Fracture toughness (KIC)	40 MPa $\sqrt{m}$
4	Paris constant (C)	$2.087136 \times 10{-11}$/cycle
5	Paris exponent (m)	3

life simulation. A uniform nodal density of (30×60) nodes is considered. An edge crack length $a = 10$ mm have been considered for this simulation. Orientation of this initial crack is kept at 40° with the horizontal axis. The boundary conditions along with other geometrical parameters are shown in Fig. 24a. Constant amplitude mechanical load of $\sigma_{max} = 100$ N/mm and $\sigma_{min} = 0$ N/mm is applied at the top edge of the plate whereas the bottom edge is constrained in y-direction. The quasi static crack growth is modelled using the REFGM algorithm which is also capable of simulating kinked cracks. With each incremental crack growth the crack path is determined and updated automatically within the algorithm. Figure 24b shows the stress (σ_{yy}) contours in the vicinity of crack tip before failure. For a particular crack configuration before failure, Fig. 24c represents the near-tip arrangement of nodes along with application of optimized quadrature criteria to determine cell for employing higher Gaussian quadrature compared to the rest of problem domain. All the boundary cells (highlighted with star) along with cells lying in the interior of circular regions are predetermined by algorithm as shown on Fig. 24c. The final fatigue life is estimated using Paris law. Fatigue life and critical crack length obtained by revamped EFG algorithm are found to be 910 *cycles* and 28.23 mm, whereas the same obtained by conventional EFGM approach are found as 918 *cycles* and 28.70 mm.

A comparison of average computational time for estimating fatigue life of cracked domain is presented in Table 13. It can be clearly observed that, for similar algorithm parameters, the proposed REFG algorithm is capable of estimating the fatigue life faster than the EFGM algorithm by about 77%. Moreover, the proposed criteria for modelling kinked crack is capable of simulating the near-tip stress field in quiet accurate and efficient manner.

9.6 Crack Emanating from Annular Disc

In order to establish the efficiency and modeling capabilities of the proposed algorithm for different domain geometry, an annular disc with a crack emanating from the inner edge is considered. The problem is simulated with both revamped element-free Galerkin method (REFGM) and conventional EFG method. Figure 25 shows an annular metallic disc ($r_i = 100$ mm and $r_o = 300$ mm) having an edge crack of length a with modulus of elasticity (E) = 200 GPa and Poisson's ratio (ν) = 0.3. A far-field stress, $\sigma = 100$ MPa is applied at the outer boundary. The domain has been discretized with a total of 666 nodes which are defined in form of concentric circles. This is achieved by defining nine equally spaced nodes along the radial direction and 77 equally spaced nodes along angular direction. The nodal distribution along with crack orientation is clearly shown in Fig. 25. The distribution of nodes is represented in Fig. 26. The initial Gaussian distribution over the annular disc is represented in Fig. 27. In order to visualize the implementation of optimized quadrature criteria, a region near the crack tip has been zoomed in and shown separately in Fig. 27. Again, the optimized quadrature criterion helps in determining the regions where a higher Gaussian quadrature will be utilized as compared to the rest of domain. These higher quadrature regions are predetermined by algorithm are highlighted with blue stars as shown in Fig. 27.

For a better understanding of the results obtained by Revamped EFG algorithm and conventional EFG method, the contours of stress components are plotted as shown in Figs. 28 and 29.

Figure 28 shows the contour of stress component σ_{xx} over the problem domain using the proposed REFGM algorithm. This contour plot shows that the crack surfaces are almost traction-free in x-direction as expected. In contrast, the stress contour of σ_{xx} generated using conventional EFGM shows a nearly zero stress level over the domain accompanied by a compressive stress zone to the opposite side of the crack as shown in Fig. 28b, which is misleading and incorrect.

Next, the stress contours of σ_{yy} are plotted and analyzed. Figure 29a presents the contour of σ_{yy} using REFGM algorithm. The crack surfaces are almost traction-free in y-direction as per theoretical expectation. A high stress level is generated at the crack tip (compared to the rest of domain), which is a unique feature of stress singularity at the crack tip. In comparison to that, EFGM is incapable of simulating the crack tip singularity as shown in Fig. 29b.
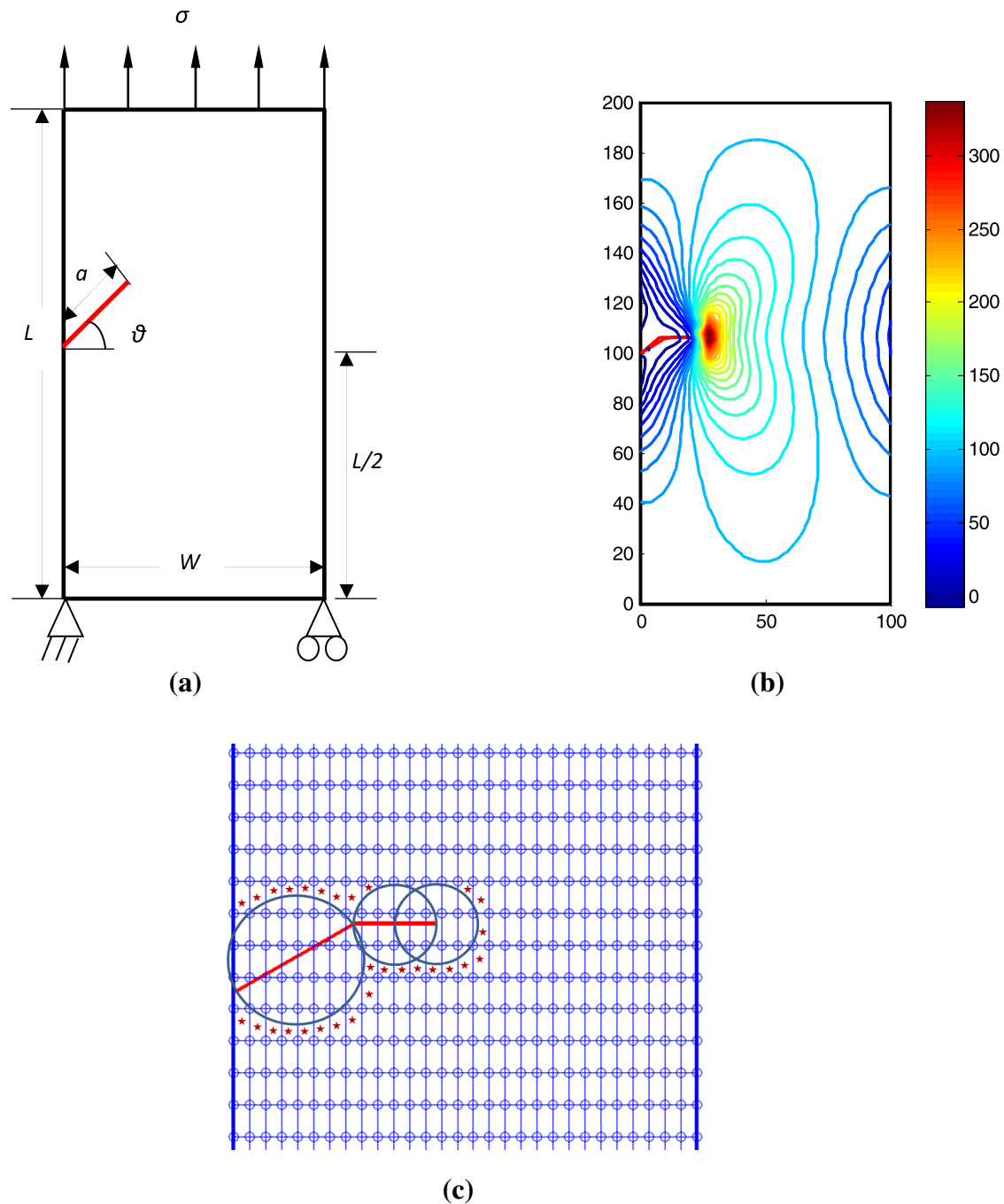
Fig. 24 Plate with inclined crack **a** problem geometry, **b** stress contours (σ_{yy}), **c** Near-tip nodes and optimized quadrature cells

The values of stress intensity factor K_I are evaluated for different crack lengths. Figure 30 shows a relative comparison of stress intensity factor (SIFs) K_I, for different crack lengths, varying from 5 to 15 mm, obtained using both revamped EFG algorithm and conventional EFGM. Both the results are compared with Finite Element Method (FEM) solution obtained using ANSYS-14 software. It can be clearly seen that for all values of crack length, the results obtained by REFGM are in good agreement with those

obtained by FEM, whereas the results obtained by conventional EFGM are absurd and deviating with the reference FEM solution.

Moreover, a comparison of average computational time for simulating crack tip field in annular disc is presented in Table 14. This computational time simulation is performed for a crack length of 12 mm. Table 14 shows that for similar algorithm parameters the proposed REFGM algorithm is capable of estimating the results faster than the EFG method

Table 13 Comparison of average simulation time for fatigue life estimation

Process parameters	Method	
	conventional EFGM	Revamped EFGM
Total number of nodes (n_d)	1800	1800
Gauss quadrature	6×6	Variable
Scaling factor (d_{max})	2	2
Area ratio	–	2
Computational time	812 s	182 s

Fig. 26 Nodal distribution over domain

by around 75% in this case. Moreover, the proposed REFGM algorithm is capable of modelling the near-tip stress field quiet accurately and efficiently along with obtaining accurate values of stress Intensity factors at the crack tip.

10 Conclusion

Element-free Galerkin method has been successfully revamped within its framework by incorporating improved moving least-square method together with blended enrichment criteria and optimized quadrature criteria. Moreover,

Fig. 25 Annular disc with an interior edge crack
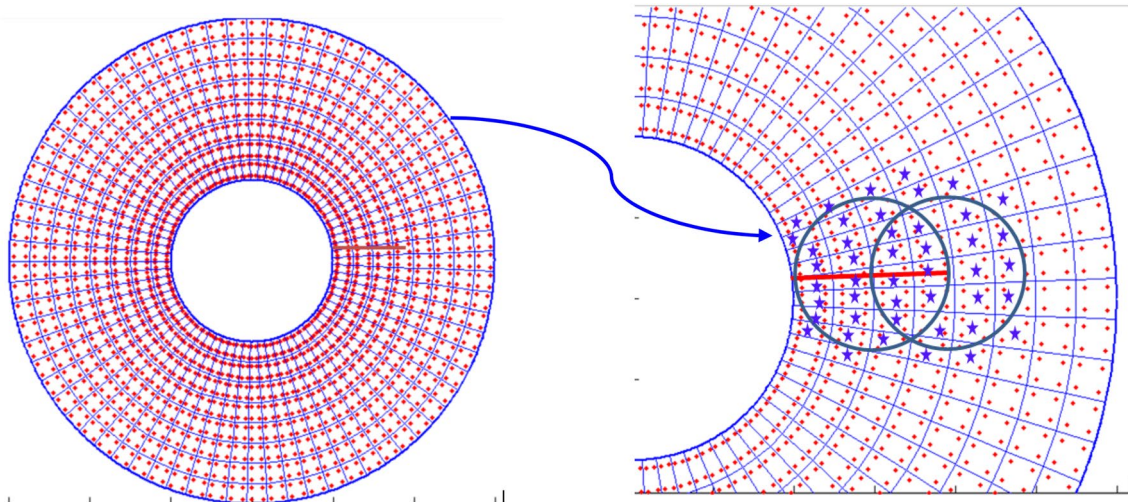
Fig. 27 Gaussian points over the domain, Optimized quadrature criteria
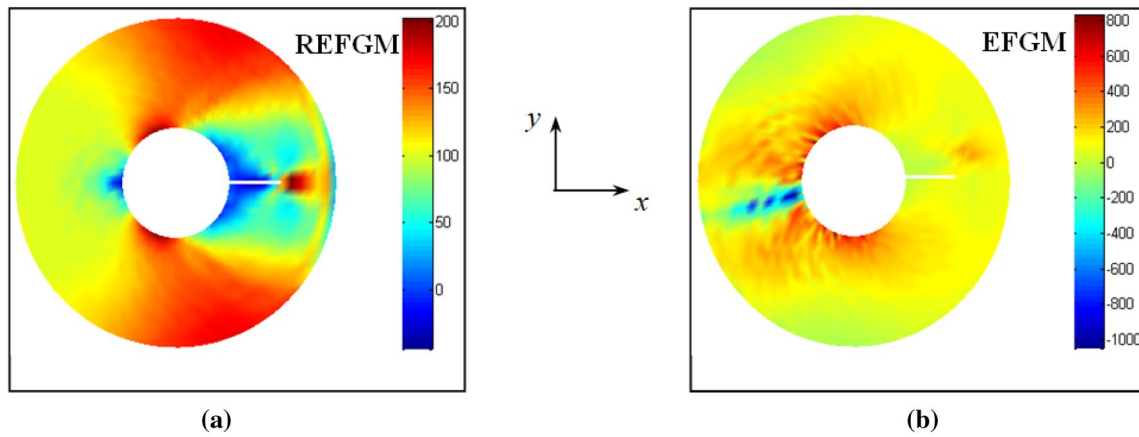
Fig. 28 Contours of stress component σ_{xx}
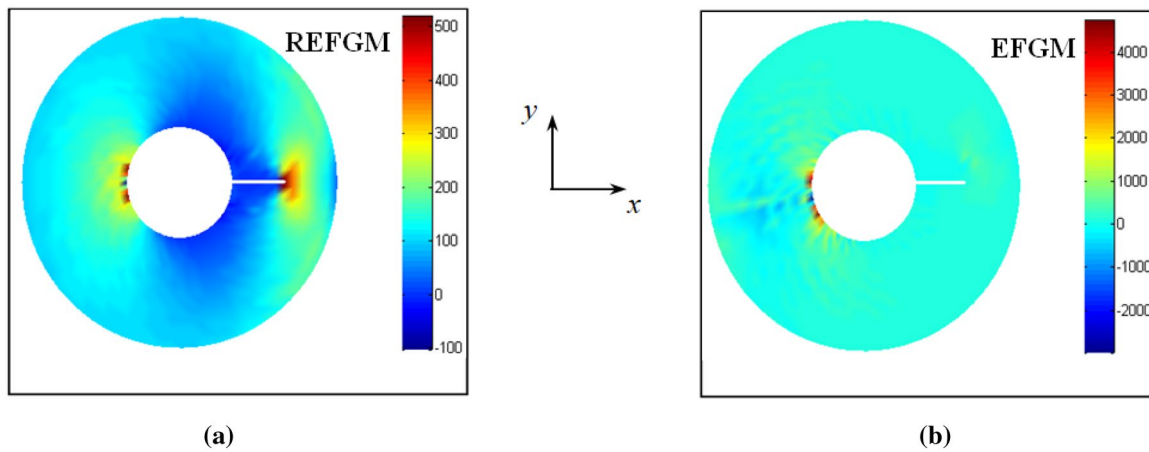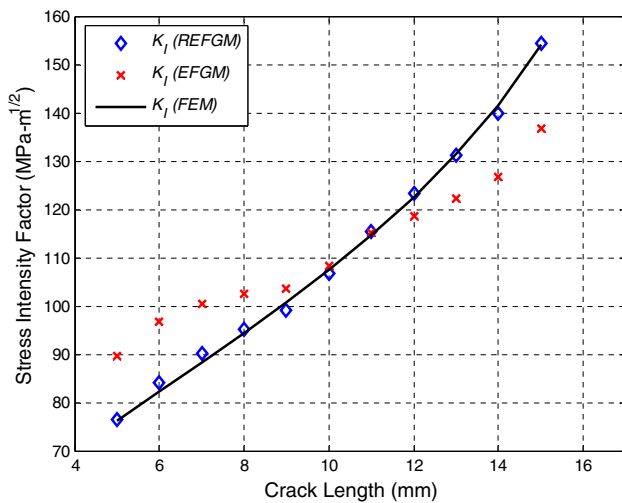

Fig. 29 Contours of stress component σ_{yy}

suitable parametric optimization has been performed for the selection of EFGM algorithm parameters thereby improving its robustness and accelerating the overall computational time of the algorithm. The revamped EFGM algorithm so developed is tested for a variety of fracture problems involving mechanical/thermal loads and compared with conventional EFGM algorithm. An average of 70–80% reduction in

Fig. 30 Stress intensity factor (K_I) values for different crack lengths

Table 14 Comparison of average simulation time for cracked annular disc

Process parameters	Method	
	conventional EFGM	Revamped EFGM
Total number of nodes (n_d)	666	666
Gauss quadrature	6×6	Variable
Scaling factor (d_{max})	2	2
Area ratio	–	2
Computational time	87 s	22 s

computational time is achieved with the proposed algorithm. The revamped EFGM algorithm outscores not only in terms of computational efficiency but also in terms of its robustness and flexibility to simulate variety of problems. The proficiency of revamped EFGM algorithm can be further extended for modelling of 3D fracture problems in complex geometries which requires the use of voluminous nodal data thereby increasing the computational time in an exponential way.

References

Afsar AM, Go J (2010) Finite element analysis of thermoelastic field in a rotating FGM circular disk. Appl Math Model 34:3309–3320. https://doi.org/10.1016/j.apm.2010.02.022

Asadpoure A, Mohammadi S, Vafai A (2006) Modeling crack in orthotropic media using a coupled finite element and partition of unity methods. Finite Elem Anal Des 42:1165–1175. https://doi.org/10.1016/j.finel.2006.05.001

Belytschko T, Lu YY, Gu L (1994a) Element free Galerkin methods. Int J Numer Methods Eng 37:229–256. https://doi.org/10.1002/nme.1620370205

Belytschko T, Gu L, Lu YY (1994b) Fracture and crack growth by element free Galerkin methods. Model Simul Mater Sci Eng 2:519–534. https://doi.org/10.1088/0965-0393/2/3A/007

Belytschko T, Organ D, Krongauz Y (1995) A coupled finite element-element-free Galerkin method. Comput Mech 17:186–195. https://doi.org/10.1007/BF00364080

Belytschko T, Lu YY, Gu L (1993) Crack propagation by element free Galerkin methods. In: Proceedings of the 1993 ASME winter annual meeting, pp 191–205

Belytschko T, Lu YY, Gu L et al (1995) Element-free Galerkin methods for static and dynamic fracture. Int J Solids Struct 32:2547–2570. https://doi.org/10.1016/0020-7683(94)00282-2

Cao Y, Yao L, Yin Y (2013) New treatment of essential boundary conditions in EFG method by coupling with RPIM. Acta Mech Solid Sin 26:302–316. https://doi.org/10.1016/S0894-9166(13)60028-2

Chao TY, Chow WK (2002) A review on the applications of finite element method to heat transfer and fluid flow. Int J Arch Sci 3:1–19

Chen J-S, Wang H-P (2000) New boundary condition treatments in meshfree computation of contact problems. Comput Methods Appl Mech Eng 187:441–468. https://doi.org/10.1016/S0045-7825(00)80004-3

Dolbow J, Belytschko T (1998) An introduction to programming the meshless element free Galerkin method. Arch Comput Methods Eng 5:207–241. https://doi.org/10.1007/BF02897874

Duflot M (2008) The extended finite element method in thermo-elastic fracture mechanics. Int J Numer Methods Eng 74:827–847. https://doi.org/10.1002/nme.2197

Elizalde-Gonzalez MP, Garcia-Diaz LE (2010) Application of a Taguchi L16 orthogonal array for optimizing the removal of acid orange 8 using carbon with a low specific surface area. Chem Eng J 163:55–61. https://doi.org/10.1016/j.cej.2010.07.040

Garg S, Pant M (2016) Numerical simulation of thermal fracture in functionally graded materials using element-free Galerkin method. Sadhana Acad Proc Eng Sci 42:417–431. https://doi.org/10.1007/s12046-017-0612-1

Garg S, Pant M (2018a) Numerical simulation of thermal fracture coatings using using element free Galerkin method. Indian J Eng Mater Sci 24:217–232. https://doi.org/10.1007/s12046-017-0612-1

Garg S, Pant M (2018b) Meshfree methods: a comprehensive review of applications. Int J Comput Methods 15:1830001-1-1830001–85. https://doi.org/10.1142/S0219876218300015

Gavete L, Falcon S, Bellido JC (2000) Dirichlet boundary conditions in element free Galerkin method. In: European congress computing methods applied science engineering, Barcelona

Günther FC, Liu WK (1998) Implementation of boundary conditions for meshless methods. Comput Methods Appl Mech Eng 163:205–230. https://doi.org/10.1016/S0045-7825(98)00014-0

He Z, Li P, Zhao G et al (2011) A meshless Galerkin least-square method for the Helmholtz equation. Eng Anal Bound Elem 35:868–878. https://doi.org/10.1016/j.enganabound.2011.01.010

Ju SH, Hsu HH (2014) Solving numerical difficulties for element-free Galerkin analyses. Comput Mech 53:273–281. https://doi.org/10.1007/s00466-013-0906-z

Kaddouri K, Belhouari M, Bouiadjra et al (2006) Finite element analysis of crack perpendicular to bi-material interface: case of couple ceramic-metal. Comput Mater Sci 35:53–60. https://doi.org/10.1016/j.commatsci.2005.03.003

Kaljevic I, Saigal S (1997) An improved element free Galerkin formulation. Int J Numer Methods Eng 40:2953–2974. https://doi.org/10.1002/(SICI)1097-0207(19970830)40:16%3c2953::AID-NME201%3e3.0.CO;2-S

Kc A, Kim JH (2008) Interaction integrals for thermal fracture of functionally graded materials. Eng Fract Mech 75(8):2542–2565. https://doi.org/10.1016/j.engfracmech.2007.07.011

Kosaraju S, Anne VG, Popuri BB (2012) Taguchi analysis on cutting forces and temperature in turning titanium Ti-6Al-4V. Int J Mech Ind Eng 1:55–59. https://doi.org/10.47893/IJMIE.2012.1068

Lancaster P, Salkauskas K (1981) Surfaces generated by moving least squares methods. Math Comput 37:141–141. https://doi.org/10.1090/S0025-5718-1981-0616367-1

Lee S-H, Yoon Y-C (2004) Numerical prediction of crack propagation by an enhanced element-free Galerkin method. Nucl Eng Des 227:257–271. https://doi.org/10.1016/j.nucengdes.2003.10.007

Li M, Werner E, You J-H (2015) Influence of heat flux loading patterns on the surface cracking features of tungsten armor under ELM-like thermal shocks. J Nucl Mater 457:256–265. https://doi.org/10.1016/j.jnucmat.2014.11.026

Liew KM, Cheng Y, Kitipornchai S (2005) Boundary element-free method (BEFM) for two-dimensional elastodynamic analysis using Laplace transform. Int J Numer Methods Eng 64(12):1610–1627. https://doi.org/10.1002/nme.1417

Liew KM, Cheng Y, Kitipornchai S (2006) Boundary element-free method (BEFM) and its application to two-dimensional elasticity problems. Int J Numer Methods Eng 65(8):1310–1332. https://doi.org/10.1002/nme.1489

Liu G, Tu Z (2002) An adaptive procedure based on background cells for meshless methods. Comput Methods Appl Mech Eng 191:1923–1943. https://doi.org/10.1016/S0045-7825(01)00360-7

Lu YY, Belytschko T, Gu L (1994) A new implementation of the element free Galerkin method. Comput Methods Appl Mech Eng 113:397–414. https://doi.org/10.1016/0045-7825(94)90056-6

Mahapatra SS, Patnaik A (2007) Optimization of wire electrical discharge machining (WEDM) process parameters using Taguchi method. Int J Adv Manuf Technol 34:911–925. https://doi.org/10.1007/s00170-006-0672-6

Miyakazi N, Ikeda T, Soda T et al (1993) Stress intensity factor analysis of interface crack using boundary element method (application of contour integral method). Eng Fract Mech 45:599–610. https://doi.org/10.1016/0013-7944(93)90266-U

Musivand-Arzanfudi M, Hosseini-toudeshky H, Musivand-Arzanfudi M (2007) Extended parametric meshless Galerkin method. Comput Methods Appl Mech Eng 196:2229–2241. https://doi.org/10.1016/j.cma.2006.11.011

Nagashima T, Omoto Y, Tani S (2003) Stress intensity factor analysis of interface cracks using X-FEMInt. J Numer Methods Eng 56:1151–1173. https://doi.org/10.1002/nme.604

Nguyen VP, Rabczuk T, Bordas S et al (2008) Meshless methods: A review and computer implementation aspects. Math Comput Simul 79:763–813. https://doi.org/10.1016/j.matcom.2008.01.003

Pant M, Bhattacharya S (2016) Fatigue crack growth analysis of functionally graded materials by EFGM and XFEM. Int J Comput Methods 14:1750004-1–1750004-33. https://doi.org/10.1142/S0219876217500049

Pant M, Singh IV, Mishra BK (2010) Numerical simulation of thermoelastic fracture problems using element free Galerkin method. Int J Mech Sci 52:1745–1755. https://doi.org/10.1016/j.ijmecsci.2010.09.008

Pant M, Singh IV, Mishra BK (2011a) A numerical study of crack interactions under thermo-mechanical load using EFGM. J Mech Sci Technol 25:403–413. https://doi.org/10.1007/s12206-010-1217-3

Pant M, Singh IV, Mishra BK (2011b) Evaluation of mixed mode stress intensity factors for interface cracks using EFGM. Appl Mater Mod 35(7):3443–3459. https://doi.org/10.1016/j.apm.2011.01.010

Pathak H (2017) Three-dimensional quasi-static fatigue crack growth analysis in functionally graded materials (FGMs) using coupled FE-XEFG approach. Theor Appl Fract Mech 92:59–75. https://doi.org/10.1016/j.tafmec.2017.05.010

Pathak H, Singh A, Singh IV (2012) Numerical simulation of bi-material interfacial cracks using EFGM and XFEM. Int J Mech Mater Des 8:9–36. https://doi.org/10.1007/s10999-011-9173-3

Pathak H, Singh A, Singh IV (2014) Fatigue crack growth simulations of homogeneous and bi-material interfacial cracks using element free Galerkin method. Appl Math Model 38:3093–3123. https://doi.org/10.1016/j.apm.2013.11.030

Pathak H, Singh A, Singh IV et al (2015) Three-dimensional stochastic quasi-static fatigue crack growth simulations using coupled FE-EFG approach. Comput Struct 160:1–19. https://doi.org/10.1016/j.compstruc.2015.08.002

Pathak H, Singh A, Singh IV (2016) Three-dimensional quasi-static interfacial crack growth simulations in thermo-mechanical environment by coupled FE-EFG approach. Theor Appl Fract Mech 86:267–283. https://doi.org/10.1016/j.tafmec.2016.08.001

Pathak H, Singh A, Singh IV (2017) Numerical simulation of 3D thermo-elastic fatigue crack growth problems using coupled FE-EFG approach. J Inst Eng Ser C 98:295–312. https://doi.org/10.1007/s40032-016-0256-7

Prasad NNV, Aliabadi MH (1994) Incremental crack growth in thermoelastic problems. Int J Fract 66:45–50. https://doi.org/10.1007/BF00042591

Rajesh KN, Rao BN (2010) Two-dimensional analysis of anisotropic crack problems using coupled meshless and fractal finite element method. Int J Fract 164:285–318. https://doi.org/10.1007/s10704-010-9496-3

Rao BN, Rahman S (2003) Mesh-free analysis of cracks in isotropic functionally graded materials. Eng Fract Mech 70:1–27. https://doi.org/10.1016/S0013-7944(02)00038-3

Reddy RM, Rao BN (2008) Continuum shape sensitivity analysis of mixed-mode fracture using fractal finite element method. Eng Fract Mech 75:2860–2906. https://doi.org/10.1016/j.engfracmech.2008.01.001

Salari-Rad H, Rahimi-Dizadji M, Rahimi-Pour S et al (2011) Meshless EFG simulation of linear elastic fracture propagation under various loadings. Arab J Sci Eng 36:1381–1392. https://doi.org/10.1007/s13369-011-0125-x

Sheng M, Li G, Shah S (2015) A modified method to determine the radius of influence domain in element-free Galerkin method. J Mech Eng Sci Part-c 229:795–805. https://doi.org/10.1177/0954406214542034

Shepard D (1968) A two-dimensional interpolation function for irregularly-spaced data. In: 23rd ACM National Conference, pp 517–524. https://doi.org/10.1145/800186.810616

Singh IV, Sandeep K, Prakash R (2003) Heat transfer analysis of two-dimensional fins using meshless element free Galerkin method. Numer Heat Transf Part A Appl 44:73–84. https://doi.org/10.1080/713838174

Sukumar N, Prevost J (2003) Modeling quasi-static crack growth with the extended finite element method part I: Computer implementation. Int J Sol Struct 40:7513–7537. https://doi.org/10.1016/j.ijsolstr.2003.08.002

Sukumar N, Huang ZY, Prevost JH et al (2004) Partition of unity enrichment for bimaterial interface cracks. Int J Numer Methods Eng 59:1075–1102. https://doi.org/10.1002/nme.902

Valencia OF, Gómez-Escalonilla FJ, Díez JL (2008) Influence of selectable parameters in element-free Galerkin method: one-dimensional bar axially loaded problem. Proc Inst Mech Eng Part C J Mech Eng Sci 222:1621–1633. https://doi.org/10.1243/09544062JMES782

Valencia OF, Gómez-Escalonilla FJ, Díez JL (2009) The influence of selectable parameters in the element-free Galerkin method: a one-dimensional beam-in-bending problem. Proc Inst Mech Eng Part C J Mech Eng Sci 223:1579–1590. https://doi.org/10.1243/09544062JMES1198

Wang H, Liu Y, Yang P et al (2016) Parametric study and optimization of H-type finned tube heat exchangers using Taguchi method. Appl Therm Eng 103:128–138. https://doi.org/10.1016/j.applthermaleng.2016.03.033

Wen PH, Aliabadi MH, Liu YW (2008) Meshless method for crack analysis in functionally graded materials with enriched radial base functions. Comput Model Eng Sci 30:133–147. https://doi.org/10.3970/cmes.2008.030.133

Wenterodt C, Von Estorff O (2011) Optimized meshfree methods for acoustics. Comput Methods Appl Mech Eng 200:2223–2236. https://doi.org/10.1016/j.cma.2011.03.011

Xuan L (2002) Meshless element-free Galerkin method in NDT applications. AIP Conf Proc 615:1960–1967. https://doi.org/10.1063/1.1473033

Yagawa G, Furukawa T (2000) Recent developments of free mesh method. Int J Numer Methods Eng 47:1419–1443. https://doi.org/10.1002/(SICI)1097-0207(20000320)47:8%3c1419::AID-NME837%3e3.0.CO;2-E

Yau JF, Wang SS, Corten HT (1980) A mixed-mode crack analysis of isotropic solids using conservation laws of elasticity. J Appl Mech 47:335–341. https://doi.org/10.1115/1.3153665

Zhang Z, Liew KM, Cheng Y et al (2008) Analyzing 2D fracture problems with the improved element-free Galerkin method. Eng Anal Bound Elem 32:241–250. https://doi.org/10.1016/j.enganabound.2007.08.012